Selective inhibition of HDAC3 targets synthetic vulnerabilities and activates immune surveillance in lymphoma.

Patrizia Mondello[1][§], Saber Tadros[2][§], Matt Teater[1], Lorena Fontan[1], Aaron Y. Chang[3], Neeraj Jain[2], Haopeng Yang[2], Shailbala Singh[4], Hsia-Yuan Ying[1], Chi-Shuen Chu[5], Man Chun John Ma[2], Eneda Toska[6], Stefan Alig[7], Matthew Durant[1], Elisa de Stanchina[8], Sreejoyee Ghosh[2], Anja Mottok[9], Loretta Nastoupil[2], Sattva S. Neelapu[2], Oliver Weigert[7], Giorgio Inghirami[10], Josè Baselga[5], Anas Younes[11], Cassian Yee[4], Ahmet Dogan[12], David A. Scheinberg[3], Robert G Roeder[5], Ari M. Melnick[1*], Michael R. Green[2,13,14*]

[1]Division of Hematology/Oncology, Department of Medicine, Weill Cornell Medical College, New York, NY 10065, USA; [2]Department of Lymphoma & Myeloma, University of Texas MD Anderson Cancer Center, Houston, TX, USA; [3]Molecular Pharmacology Program, Memorial Sloan Kettering Cancer Center, New York, NY, USA; [4]Department of Melanoma Medical Oncology, University of Texas MD Anderson Cancer Center; [5]Laboratory of Biochemistry and Molecular Biology, The Rockefeller University, New York, NY, USA; [6]Department of Human Oncology and Pathogenesis, Memorial Sloan Kettering Cancer Center, New York, NY, USA; [7]Department of Internal Medicine III, University Hospital of the Ludwig-Maximilians-University Munich, Munich, Germany; [8]Antitumor Assessment Core Facility, Memorial Sloan Kettering Cancer Center, New York, NY 10065, USA; [9]Institute of Pathology, University of Würzburg and Comprehensive Cancer Center Mainfranken, Würzburg, Germany; [10]Department of Pathology and Laboratory Medicine, Weill Cornell Medical College, New York, NY, USA; [11]Department of Medicine, Memorial Sloan Kettering Cancer Center, New York, NY, USA; [12]Departments of Pathology and Laboratory Medicine, Memorial Sloan Kettering Cancer Center, New York, NY, USA; [13]Department of Genomic Medicine, University of Texas MD Anderson Cancer Center, Houston, TX, USA; [14]Center for Cancer Epigenetics, University of Texas MD Anderson Cancer Center, Houston, TX, USA.
[§]Equally contributed first authors. *Equally contributed senior authors.

Corresponding Authors:
Michael R. Green, Ph.D.
Department of Lymphoma & Myeloma and Department of Genomic Medicine,
University of Texas MD Anderson Cancer Center,
Houston, TX, 77030.
Email: mgreen5@mdanderson.org

Ari Melnick, MD
Department of Medicine, Weill Cornell Medicine,
413 East 69th Street,
New York, NY, 10021.
Email: amm2014@med.cornell.edu

Key words: CREBBP, HDAC3, Interferon, MHC class II

Running Title: Targeting HDAC3 in lymphoma

56 Pharmaceuticals. J.B. also has performed consulting and/or advisory work for Grail, PMV Pharma, ApoGen,
57 Juno, Lilly, Seragon, Novartis, and Northern Biologics, and he has stock or other ownership interests in
58 PMV Pharma, Grail, Juno, Varian, Foghorn, Aura, Infinity Pharmaceuticals, ApoGen, as well as Tango and
59 Venthera, of which is a co-founder. He has previously received honoraria or travel expenses from Roche,
60 Novartis, and Eli Lilly. AMM receives research funding from Janssen and Daiichi SAnkyo, is a consultant
61 for Epizyme and Constellation, and is an advisory board member for KDAc Therapeutics. MRG is a
62 consultant to VeraStem Oncology and has stock ownership interest in KDAc Therapeutics.

63

64

65

66

67

68

69

70

71

72

73

74

75

76

77

78

79

80

81

82

83 *CREBBP* mutations are highly recurrent in B-cell lymphomas and either inactivate its

84 histone acetyltransferase (HAT) domain or truncate the protein.   Herein, we show that

85 these two classes of mutations yield different degrees of disruption of the epigenome,

86 with HAT mutations being more severe and associated with inferior clinical outcome.

87 Genes perturbed by *CREBBP* mutation are direct targets of the BCL6/HDAC3 onco-

88 repressor complex.   Accordingly, we show that HDAC3 selective inhibitors reverse

89 *CREBBP* mutant aberrant epigenetic programming resulting in: a) growth inhibition of

90 lymphoma cells through induction of BCL6 target genes such as *CDKN1A* and b)

91 restoration of immune surveillance due to induction of BCL6-repressed IFN pathway and

92 antigen presentation genes.   By reactivating these genes, exposure to HDAC3 inhibitor

93 restored the ability of tumor infiltrating lymphocytes to kill DLBCL cells in an MHC class I

94 and II dependent manner, and synergized with PD-L1 blockade in a syngeneic model *in*

95 *vivo*. Hence HDAC3 inhibition represents a novel mechanism-based immune-epigenetic

96 therapy for *CREBBP* mutant lymphomas.

97

98

99

100 **STATEMENT OF SIGNIFICANCE**

101 We have leveraged the molecular characterization of different types of *CREBBP*

102 mutations to define a rational approach for targeting these mutations through selective

103 inhibition of HDAC3. This represents an attractive therapeutic avenue for targeting

104 synthetic vulnerabilities in *CREBBP* mutant cells in tandem with promoting anti-tumor

105 immunity.

INTRODUCTION

Diffuse large B-cell lymphoma (DLBCL) and follicular lymphoma (FL) are the two most frequent subtypes of non-Hodgkin lymphoma. These diseases originate from germinal center B (GCB)-cells; a stage of development that naturally allows for the proliferation and affinity maturation of antigen-experienced B-cells to produce terminally-differentiated memory B-cells or plasma cells. The germinal center (GC) reaction is regulated by B-cell-intrinsic activation and suppression of genes by master regulators such as the BCL6 transcription factor[1], and extrinsically via the interaction of GCB-cells with follicular helper T (T_{FH})-cells and other immune cells within the GC[2]. The BCL6 transcription factor is critical for GCB-cell development and coordinately suppresses the expression of large sets of genes by recruiting SMRT/NCOR co-repressor complexes containing HDAC3[3], the LSD1 histone demethylase[4], and tethering a non-canonical polycomb repressor 1-like complex in cooperation with EZH2[5]. These genes are normally reactivated to drive GC exit and terminal differentiation in the GC light zone, but the epigenetic control of these dynamically-regulated GC transcriptional programs is perturbed in DLBCL and FL via the downstream effects of somatic mutation of chromatin modifying genes[6] (CMG).

The second most frequently mutated CMG in both DLBCL and FL is the *CREBBP* gene, which encodes a histone acetyltransferase that activates transcription via acetylation of histone H3 lysine 27 (H3K27Ac) and other residues. We have previously found that these mutations arise as early events during the genomic evolution of FL and reside in a population of tumor propagating cells, often referred to as common progenitor cells (CPCs)[7]. We have also noted an association between *CREBBP* inactivation and reduced

129   expression of MHC class II in human and murine lymphomas[7,8]. The expression of MHC

130   class II is critical for the terminal differentiation of B-cells through the GC reaction[9]. The

131   interaction with helper T-cells via MHC class II results in B-cell co-stimulation through

132   CD40 that drives NFκB activation and subsequent IRF4-driven suppression of BCL6.

133   However, in B-cell lymphoma, tumor antigens may also be presented in MHC class II and

134   recognized by CD4 T-cells that drive an anti-tumor immune response[10,11]. The active

135   suppression of MHC class II expression in B-cell lymphoma may therefore be driven by

136   evolutionary pressure against MHC class II-binding tumor antigens, as recognized in

137   other cancers[12]. In support of this notion, the reduced expression of MHC class II has

138   been found to be associated with poor outcome in DLBCL[13,14].

139

140   Recently, MHC class II expression has been defined as an important component of

141   interferon-gamma (IFN-γ) related signatures that are predictive of the activity of PD-1

142   neutralizing antibodies[14-17]. This is consistent with a prominent role for CD4 T-cells in

143   directing anti-tumor immunity and responses to immunotherapy[18]. Despite this, current

144   immunotherapeutic strategies largely rely on the pre-existence of an inflammatory

145   microenvironment for therapeutic efficacy. Here, we have characterized the molecular

146   consequences of *CREBBP* mutations and identified BCL6-regulated cell cycle,

147   differentiation, and IFN signaling pathways as core features that are aberrantly silenced

148   at the epigenetic and transcriptional level. We show that HDAC3 inhibition specifically

149   restores these pathways thus suppressing growth and most critically enabling T-cells to

150   recognize and kill lymphoma cells. Together, these highlight multiple mechanisms by

151   which selective inhibition of HDAC3 can drive tumor-intrinsic killing as well as activate

152 IFN-γ signaling and anti-tumor immunity which extends to both *CREBBP* wild-type and

153 *CREBBP* mutant tumors.

154

155 **<u>RESULTS</u>**

156 **_CREBBP[R1446C]_ mutations function in a dominant manner to suppress BCL6 co-**

157 **regulated epigenetic and transcriptional programs.**

158 In B-cell lymphomas, the *CREBBP* gene is predominantly targeted by point mutations

159 that result in single amino acid substitutions within the lysine acetyltransferase (KAT)

160 domain[7,19], with a hotspot at arginine 1446 (R1446) that leads to a catalytically inactive

161 protein[20,21]. However, all of the prior studies characterizing the effects of *CREBBP*

162 mutation have been performed using knock-out or knock-down of *Crebbp*, resulting in

163 loss-of-protein (LOP)[8,19,22-25]. Furthermore, mutations of R1446 have not been

164 documented in any lymphoma cell line. We therefore opted to investigate whether there

165 may be unique functional consequences of KAT domain hotspot mutations of *CREBBP*.

166 To achieve this, we utilized CRISPR/Cas9-mediated gene editing with two unique guide-

167 RNAs (gRNA) to introduce the most common *CREBBP* mutation, R1446C, into a

168 *CREBBP* wild-type cell line bearing the t(14;18)(q21;q32) translocation, RL (**Figure 1A**).

169 This allowed us to generate clones from each gRNA that had received the constructs but

170 remained wild-type (*CREBBP[WT]*), those that edited their genomes to introduce the point

171 mutations into both alleles (*CREBBP[R1446C]*), and those that acquired homozygous

172 frameshift mutations resulting in LOP (*CREBBP[KO]*) (**Figure S1**). These isogenic sets of

173 clones differ only in their *CREBBP* mutation status, and therefore allow for detailed

174 functional characterization in a highly controlled setting.

175

176   Western blot confirmed that the CREBBP^{R1446C} protein was still expressed and that

177   *CREBBP^{KO}* mutations resulted in a complete loss of protein expression (**Figure 1B**).

178   Western blot with densitometry of the H3K27Ac mark revealed significant reduction in

179   H3K27Ac in *CREBBP^{R1446C}* cells vs isogenic *CREBBP^{WT}* controls (p<0.001; **Figure 1C**).

180   Although *CREBBP^{KO}* cells also showed lower H3K27Ac abundance than isogenic

181   *CREBBP^{WT}* controls, this reduction was not statistically significant (p=0.106). We

182   performed chromatin immunoprecipitation (ChIP)-sequencing for H3K27Ac to define the

183   physical location of these changes and identify potentially deregulated genes. This

184   revealed 2,022 regions with significantly reduced acetylation, and 2,304 regions with

185   significantly increased acetylation in *CREBBP^{R1446C}* cells compared to isogenic

186   *CREBBP^{WT}* controls (Fold change >1.5, Q-value<0.01; **Figure 1D and S2**, **Table S1**).

187   This pattern was mirrored by another CREBBP-catalyzed mark, H3K18Ac, and the loss

188   or gain of histone acetylation was also accompanied by gain or loss of H3K27me3,

189   respectively (**Figure S3A-D**). Regions with loss of H3K27Ac were observed to normally

190   bear this mark in human GCB cells[24] (**Figure 1D**), suggesting that *CREBBP^{R1446C}*

191   mutations lead to loss of a normal GCB epigenetic program. Notably, *CREBBP^{KO}* resulted

192   in a reduction of H3K27Ac in these regions also, but at a lower magnitude than that

193   observed with *CREBBP^{R1446C}* mutations (**Figure 1D-E**). This was not observed for regions

194   with increased H3K27Ac, which showed little change in *CREBBP^{KO}* cells.

195

196   Using RNA sequencing, we observed broad changes in transcription, with 766 genes

197   showing significantly increased expression and 733 genes showing significantly

198 decreased expression in *CREBBP*^{R1446C} cells compared to *CREBBP*^{WT} isogenic controls

199 (Fold change >1.5, Q-value<0.01; **Figure 1F**; **Table S2**). The genes that were proximal

200 to regions of H3K27Ac loss showed a coordinate reduction in transcript abundance and

201 *vice versa* (FDR<0.001, **Figure 1G**), suggesting that these broad changes in transcription

202 are directly linked to altered promoter/enhancer activity as a result of differential

203 H3K27Ac. Importantly, we observed significant enrichment of the transcriptional signature

204 induced by shRNA knock-down of *CREBBP* in murine B-cells or human DLBCL cell lines[8]

205 (**Figure 1H**). However, an even more significant enrichment was observed for the

206 signature of genes we defined as being lost in association with *CREBBP* mutation in

207 primary human *CREBBP* mutant FL B-cells[7] (FDR<0.001, **Figure 1H**). Consistent with

208 our CRISPR cell line results, primary FL B-cells with *CREBBP* LOP mutations were

209 observed to have significantly less repression of this signature by single sample gene set

210 enrichment analysis (ssGSEA) compared to those with *CREBBP* KAT domain mutation

211 (P = 0.039; **Figure S4**).

212

213 We used epigenetic and transcriptional profiles and hypergeometric analysis to gain

214 insight into biological functions disrupted by *CREBBP*^{R1446C} mutations (**Figure 1I**, **Table**

215 **S3-4**). This confirmed a significant enrichment of genes downregulated in *CREBBP*

216 mutant lymphoma patients, and further revealed an enrichment of BCL6-SMRT and BCL6

217 targets, consistent with the proposed role of CREBBP in opposing BCL6 mediated

218 transcriptional repression.   The biological functions of these genes included B-cell

219 receptor (BCR) and NFκB signaling in addition to interferon signaling and antigen

220 presentation (**Figure 1I**). In line with the enrichment of antigen presentation pathways

221   and the genome-wide differences in H3K27Ac patterning, we observed more severe

222   reduction of H3K27Ac over the MHC class II locus in *CREBBP*^{R1446C} vs *CREBBP*^{KO} cells

223   (**Figure 1J**). This was associated with a ~2-fold reduction of cell surface MHC class II in

224   *CREBBP*^{KO} cells compared to isogenic *CREBBP*^{WT} controls, but a ~37-fold reduction in

225   *CREBBP*^{R1446C} cells (**Figure 1K**). Notably, EP300 is expressed at a high level in all of the

226   CRISPR modified cell lines and ChIP-qPCR showed that the MHC class II locus is bound

227   by both CREBBP and EP300 in these cells (**Figure S5A-C**). Moreover, inhibition of

228   EP300 activity in *CREBBP*^{KO} cells reduced the expression of MHC class II to levels similar

229   to that in *CREBBP*^{R1446C} cells (**Figure S5D**), suggesting that the redundant activity of

230   EP300 may partially sustain MHC class II expression in *CREBBP*^{KO} cells. These data

231   further support a stronger epigenetic and transcriptional suppression of BCL6 target

232   genes, including those involved in antigen presentation, with *CREBBP*^{R1446C} mutations

233   compared to *CREBBP*^{KO}.

234

235   To confirm that the *CREBBP* KAT mutation is biologically active in primary GC B-cells in

236   a similar manner to that observed in CRISPR engineered cell lines, we generated a novel

237   genetically engineered mouse model with cre-inducible expression of *Crebbp*^{R1447C}

238   (equivalent to human R1446C). The endogenous *Crebbp* locus was engineered to switch

239   from wild-type to mutant gene expression using a floxed inversion cassette (**Figure S6A**).

240   These animals were crossed to mice engineered for the Cγ1-cre allele to specifically

241   induce recombination in GC B-cells and bone marrow transplanted into irradiated CD45.1

242   recipients (**Figure S6B and C**). Transplanted mice were immunized with sheep red blood

243   cells and sacrificed 10 days later when the GC reaction is at its peak (**Figure S6C**),

244 whereupon flow cytometry was performed to assess B-cell populations. As expected,

245 there was no perturbation of earlier stages of B-cell development (**Figure S6D and E**).

246 Cre recombination was validated in sorted GC B-cells (**Figure S6F**).

247 *Cγ1Cre;Crebbp^{R1447C/+}* GC B-cells showed significantly reduced MHC class II expression

248 compared to *Cγ1Cre;Crebbp^{+/+}* controls (P=0.02, **Figure S6G),** whereas (as expected)

249 there was no difference in MHC II among naïve B-cells from either genotype (**Figure**

250 **S6H**). Finally, *Cγ1Cre;Crebbp^{R1447C/+}* mice manifested significantly skewed light-

251 zone:dark-zone ratio in favor of increased dark-zone cells (P=0.01; **Figure S6I-L**), which

252 are the cells that most reflect the actions of BCL6, although the overall abundance of GC

253 B-cells was not increased (**Figure S6M and N**). These results confirm in primary cells

254 our MHC class II findings from CRISPR/Cas9-edited clones and hence their value as a

255 platform for mechanistic studies.

256

257 Finally, mutations of *CREBBP* have been previously associated with adverse outcome in

258 FL and are incorporated into the M7-FLIPI prognostic index[26]. However, in these

259 analyses, all *CREBBP* mutations were considered collectively without discriminating

260 between KAT domain point mutations or nonsense/frameshift LOP mutations. We

261 therefore re-evaluated these data in light of our observed functional differences between

262 these mutations. This showed that there was a significant difference in failure-free survival

263 (**Figure 1L**) between these two classes of *CREBBP* mutations. This was not significant

264 for overall survival (**Figure 1M**). Specifically, patients bearing KAT domain point

265 mutations in *CREBBP* (22% of which were R1446 mutations) had a significantly reduced

266 failure-free survival compared to patients with LOP mutations in *CREBBP* (Log-Rank

267 P=0.026), with no other clinical factors being significantly different between these groups

268 (**Table S5**).   Collectively, these results provide the first direct experimental description of

269 the role of $CREBBP^{R1446C}$ mutations in lymphoma B-cells.   Our data suggest that

270 $CREBBP$ KAT domain mutations may have a potential dominant repressive function on

271 loci that can be targeted by redundant acetyltransferases, thereby driving a more

272 profound molecular phenotype that is associated with a worse patient outcome.

273

274 **Synthetic dependence on HDAC3 in *CREBBP*-mutant DLBCL is independent of**

275 **mutation subtype.**

276 Our genomic analysis showed that BCL6 target genes were significantly enriched

277 amongst those with reduced H3K27Ac and gene expression in $CREBBP^{R1446C}$ cells. We

278 therefore evaluated CREBBP and BCL6 binding over these regions using data from

279 normal GC B-cells[24] and found that the regions with $CREBBP^{R1446C}$ mutation-associated

280 H3K27Ac loss are bound by both proteins at significantly higher levels than H3K27Ac

281 peaks that remain unchanged with $CREBBP$ mutation (CREBBP Wilcoxon P=1.2^{-41},

282 BCL6 Wilcoxon P=2.83^{-52}) or peaks with increased H3K27Ac in $CREBBP^{R1446C}$ mutants

283 (CREBBP Wilcoxon P=3.01^{-137}, BCL6 Wilcoxon P=3.17^{-128}; **Figure 2A**). This suggests

284 that these genes may be antagonistically regulated by CREBBP and BCL6, the latter of

285 which mediates gene repression via recruitment of HDAC3-containing NCOR/SMRT

286 complexes[3,27]. The epigenetic suppression of gene expression in $CREBBP$ mutant cells

287 may therefore be dependent upon HDAC3-mediated suppression of BCL6 target genes.

288 Using a selective HDAC3 inhibitor, BRD3308[28], we found that $CREBBP^{R1446C}$ and

289 $CREBBP^{KO}$ clones showed greater sensitivity to HDAC3 inhibition compared to isogenic

290   WT controls in cell proliferation assays (**Figure 2B**). We confirmed this as being an on-

291   target effect of BRD3308 by performing shRNA knock-down of *HDAC3* and observing a

292   greater effect on cell proliferation in *CREBBP^{R1446C}* cells compared to isogenic controls

293   (**Figure 2C and S7**).   Moreover, HDAC3 inhibition was able to efficiently promote the

294   accumulation of H3K27Ac in a dose-dependent manner in both *CREBBP^{WT}* and

295   *CREBBP^{R1446C}* cells, as compared to the inactive chemical control compound BRD4097

296   (**Figure 2D**).   This suggests that the increased sensitivity to HDAC3 inhibition in

297   *CREBBP^{R1446C}* cells may be linked with an acquired addiction to an epigenetic change

298   driven by *CREBBP* mutation.   We posited that one of these effects may be the

299   suppression of p21 (*CDKN1A*) expression, which is a key BCL6 target gene[29] that has

300   reduced levels of H3K27Ac in both *CREBBP^{R1446C}* and *CREBBP^{KO}* cells (**Figure 2E**).   In

301   support of this, we observed a marked induction of p21 expression by BRD3308 (**Figure**

302   **2F**) and observed that shRNA-mediated silencing of p21 partially rescued the effect of

303   BRD3308 on cell proliferation (**Figure 2G**).   Therefore *CREBBP* mutations, regardless of

304   type, sensitize cells to the effects of HDAC3 inhibition in part via the induction of p21.

305

306   We aimed to confirm this trend using a larger panel of DLBCL cell lines with either WT

307   (n=6) or mutant *CREBBP* (n=6). This revealed a significantly lower ED50 to BRD3308 in

308   *CREBBP* mutant compared to WT cell lines (p=0.002, **Figure 2H-I**). We did not observe

309   this trend using the non-specific HDAC inhibitors, Romidepsin and SAHA (**Figure S8**).

310   Notably, none of these cell lines harbor KAT domain missense mutations of *CREBBP*,

311   providing further evidence that sensitivity to HDAC3 selective inhibition is independent of

312   mutation type (i.e. KAT domain missense vs nonsense/frameshift). Furthermore, we also

313   observed the induction of p21 expression and apoptosis in *CREBBP* wild-type cell lines,

314   although to a lesser degree (**Figure S9**). To gain greater insight into this, we performed

315   RNA-sequencing of *CREBBP* wild-type (OCI-Ly1) and mutant (OCI-Ly19, OZ) cell lines

316   treated with BRD3308. Notably, the ability of HDAC3 inhibition to induce the expression

317   of genes involved in the terminal differentiation of B-cells was conserved in both wild-type

318   and mutant cell lines (**Figure 2J**). These results are consistent with the role of BCL6 in

319   controlling checkpoints, terminal differentiation and other functions[1] and points towards

320   induction of these transcriptional programs as contributing to the anti-lymphoma response

321   induced by HDAC3-inhibition in both the *CREBBP* WT and mutant settings. Although

322   targetable by HDAC3 inhibition in wild-type cells, the BCL6-HDAC3 target gene set is

323   more significantly perturbed in the context of *CREBBP* mutation leading to an enhanced

324   cell-intrinsic effect of HDAC3 inhibition.

325

326   **HDAC3 inhibition is active against primary human DLBCL**

327   Our observation that HDAC3 inhibition can affect both *CREBBP* mutant and wild-type B-

328   cells led us to test its efficacy in primary patient-derived xenograft (PDX) models of

329   DLBCL. To achieve this, we first expanded *CREBBP* wild-type tumors *in vivo* and

330   transitioned them to our novel *in vitro* organoid system for exposure to BRD3308[30]. All

331   tumors that were tested showed a dose-dependent reduction in cell viability when cultured

332   with BRD3308, compared to the vehicle control (**Figure 3A**). We therefore treated 3 of

333   these *CREBBP* wild-type tumors *in vivo* with either 25mg/kg or 50mg/kg of BRD3308,

334   which led to a significant reduction in growth of PDX tumors treated with either dose

335   compared to vehicle control (**Figure 3B**). We were only able to obtain a single primary

336   human *CREBBP* mutant (R1446C) DLBCL PDX model, which could only be grown by

337   renal capsule implantation. Treatment of these tumors with 25mg/kg BRD3308 and

338   monitoring by weekly magnetic resonance imaging (**Figure 3C**) showed a significant

339   reduction in growth compared to vehicle control treated tumors (**Figure 3D**). In line with

340   our cell line models, quantitative PCR analysis of treated PDX tumors showed an

341   induction of BCL6 target genes with a role in B-cell terminal differentiation, including *IRF4*,

342   *PRDM1*, *CD138* and *CD40* compared to vehicle-treated tumors (**Figure S10**).Therefore,

343   selective inhibition of HDAC3 may be a rational approach for targeting the aberrant

344   epigenetic silencing of BCL6 target genes in primary human B-cell lymphoma.

345

346   **Selective inhibition of HDAC3 reverts the molecular phenotype of *CREBBP***

347   **mutations.**

348   We aimed to take a deeper look at the molecular consequences of HDAC3 inhibition by

349   performing H3K27Ac ChIP-seq and RNA-seq of $CREBBP^{R1446C}$ mutant cells after

350   exposure to BRD3308, as compared to the inactive negative control compound

351   BRD4097. This showed that selective HDAC3 inhibition promoted the gain of H3K27Ac

352   over a broad number of regions (n=6756, **Figure 4A**).   Strikingly, HDAC3 inhibition

353   significantly either restored or further increased the abundance of H3K27Ac at 28%

354   (558/1975) of sites that became deacetylated in $CREBBP^{R1446C}$ (hypergeometric

355   enrichment P = 3.02^{-178}), consistent with the role of HDAC3 in opposing CREBBP

356   functions (**Figure 4B**). Indeed, a more quantitative analysis indicated HDAC3 inhibition

357   coordinately increased the level of H3K27Ac over the same loci that showed reduced

358   levels in $CREBBP^{R1446C}$ compared to $CREBBP^{WT}$ cells, although this restoration of

359   H3K27Ac was not sufficient to completely revert the epigenomes of *CREBBP^R1446C* cells

360   to the level that was observed in *CREBBP^WT* cells (**Figure 4C**). In line with the role of

361   HDAC3 and BCL6 in transcriptional repression, BRD3308 induced an expression profile

362   that was markedly skewed towards gene upregulation (n=1467 vs 208 genes

363   downregulated; **Figure 4D**; **Table S6-7**), including interferon-responsive genes such as

364   antigen presentation machinery and PD-L1 (*CD274*). Notably, the genes with increased

365   expression following HDAC3 inhibition were significantly enriched for those that lose

366   H3K27Ac in *CREBBP^R1446C* compared to WT (FDR<0.001, **Figure 4E**), further supporting

367   the conclusion that HDAC3 inhibition directly counteracts changes associated with

368   *CREBBP* mutation. A quantitative assessment of ChIP-seq signal indicated that

369   enhancers manifested greater gain of H3K27Ac as compared to promoters in cells

370   exposed to HDAC3i (Wilcoxon P<0.001; **Figure 4F**), although MHC class II genes also

371   showed coordinate increases in promoter H3K27Ac (**Figure 4G**). Analysis of critical gene

372   loci that are deregulated by *CREBBP* mutation, such as the MHC class II gene cluster

373   and CIITA, exemplify this induction of H3K27ac (**Figure 4H-I**). We validated the increased

374   H3K27Ac and expression of these genes in independent experiments wherein

375   *CREBBP^R1446C* or isogenic control cells were treated with BRD3308 or vehicle, H3K27Ac

376   was measured by ChIP-qPCR (**Figure S11**), and transcript abundance measured by

377   qPCR (P<0.001, **Figure 4J**). We further validated that this was an on-target effect of

378   BRD3308 by performing shRNA-mediated knock-down of HDAC3, which resulted in the

379   increased expression of these genes relative to control shRNA (**Figure 4K**). Together

380   these data indicate that the aberrant mutant-*CREBBP* epigenetic and transcriptional

381   program can be restored by selective pharmacologic inhibition of HDAC3.

382

HDAC3 inhibition counteracts BCL6 target gene repression in lymphoma cells including IFN response, irrespective of *CREBBP* mutation status.

IFN signaling and antigen presentation genes have not been well investigated as downstream targets of BCL6-HDAC3 complexes, but were enriched in genes suppressed by *CREBBP* mutation and restored by HDAC3 inhibition. Given their critical role in anti-tumor immunity, we evaluated whether HDAC3 inhibition may be sufficient to restore or promote the expression of these BCL6-repressed immune signatures. Using MHC class II protein expression on *CREBBP[R1446C]* mutant cells as a proxy for the CREBBP/BCL6 counter-regulated IFN signaling pathway, we evaluated the activity of HDAC inhibitors for promoting the expression of immune response genes. Although HDAC inhibitors with broader specificities were able to induce MHC class II expression, selective inhibition of HDAC3 was sufficient for the robust and maximal (>10-fold) restoration of MHC class II expression in *CREBBP[R1446C]* cells (**Figure 5A and S12**) in line with our observation that these genes are silenced by BCL6/HDAC3 complexes. These selective inhibitors each show some inhibition of other HDACs[28], and their activity in opposing BCL6 function may in part be linked to inhibition of HDAC1/2 which are recruited by BCL6 via CoRest and NuRD[4,31,32]. However, HDAC1/2 have important functions in normal hematopoiesis[33], and hence compounds that target these enzymes induce toxic effects against these cells that are not elicited by BRD3308[29], suggesting that selective inhibition of HDAC3 may limit hematological toxicities that are observed with pan-HDAC inhibitors. Furthermore, while some of the less specific HDAC inhibitors were toxic to normal human CD4 and CD8 T-cells, the selective inhibition of HDAC3 was not (**Figure 5B and S13**). This suggests that

405 selective HDAC3 inhibition may be capable of eliciting immune responses by on-target

406 on-tumor induction of antigen presentation without on-target off-tumor killing of T-cells.

407

408 Based upon our observations with MHC class II, the magnitude of this induction appeared

409 to be dependent upon the baseline of expression. We therefore hypothesized that

410 *CREBBP* mutation status may determine the baseline expression for IFN and antigen

411 presentation pathways, but may not be a prerequisite for this response due to the

412 conserved activity of BCL6/HDAC3 in regulating this axis in WT cells. We

413 comprehensively evaluated this theory using our RNA-seq data from *CREBBP^{WT}* and

414 *CREBBP^{R1446C}* cells treated with either the HDAC3 inhibitor, BRD3308, or inactive control

415 compound, BRD4097. Consistent with our observations of MHC class II protein

416 expression, BRD3308 treatment coordinately induced the transcript expression of MHC

417 class II and IFN pathway genes in both *CREBBP^{WT}* and *CREBBP^{R1446C}* CRISPR-edited

418 cells (**Figure 5C**). This trend included a significant enrichment for the genes that were

419 epigenetically suppressed in association with *CREBBP* mutations, resulting in their

420 significant increase in expression in *CREBBP^{WT}* cells (**Figure 5D**) similar to our

421 observations from *CREBBP^{R1446C}* cells (**Figure 4E**).   Moreover, we observed similar

422 enrichment of transcriptionally-induced pathways in both *CREBBP^{WT}* and *CREBBP^{R1446C}*

423 cells that included the same pathways that were suppressed by *CREBBP* mutation

424 (**Figure 5E**; **Tables S7, S8, S9 and S10**). Consistent with the almost exclusive function

425 of HDAC3 as a BCL6 corepressor in GC B-cells[3], and the importance of BCL6 activity in

426 both *CREBBP* WT and mutant cells, we observed highly significant enrichment for genes

427 regulated by BCL6-SMRT complexes among genes with induced H3K27Ac and

428 expression after BRD3308 treatment (**Figure 5E**). Also significantly enriched were

429 canonical BCL6 target gene sets such as p53 regulated genes, and signaling through

430 BCR, CD40 and cytokines like IL4 and IL10. Finally we observed significant enrichment

431 for BCL6 target gene sets linked to IFN signaling, antigen presentation via MHC class II

432 and PD1 signaling.

433

434 Although there were conserved patterns of gene activation in both $CREBBP^{WT}$ and

435 $CREBBP^{R1446C}$ cells, we observed that the magnitude of this induction was greatest in

436 $CREBBP^{R1446C}$ cells, which started from a lower baseline of expression linked to mutation-

437 associated epigenetic suppression (**Figure 5F**). We identified IRF1 as a BCL6-regulated

438 transcription factor that is critical for interferon responses, and is induced by HDAC3

439 inhibition $CREBBP^{WT}$ and $CREBBP^{R1446C}$ cells (**Figure 5C**). We therefore hypothesized

440 that IRF1 may contribute to the different magnitude of induction in MHC class II genes

441 following HDAC3 inhibition in these two genetic contexts. We investigated this by

442 measuring IRF1 activity in a luciferase reporter assay in $CREBBP^{WT}$ and $CREBBP^{R1446C}$

443 mutant cells. Treatment of $CREBBP^{R1446C}$ cells with BRD3308 led to a significant

444 increase of IRF1 activity that was similar in magnitude to that induced by IFN-γ treatment

445 (**Figure 5G**). In contrast, this effect was not observed in isogenic $CREBBP^{WT}$ control cells

446 following HDAC3 inhibition, despite these cells showing similarly increased IRF1 activity

447 in response to IFN-γ treatment. Exposing $CREBBP^{R1446C}$ cells to IFN-γ neutralizing

448 antibodies only partially ameliorated MHC class II induction after BRD3308 in $CREBBP$

449 mutant cells (**Figure 5H**). This suggests that preferential induction of antigen

450 presentation by HDAC3 inhibition in $CREBBP$ mutant cells likely depends on a

451   combination of mechanisms, including directly opposing BCL6 repression of these genes

452   as well as secondary induction through IFN-γ signaling (which is also directly regulated

453   by BCL6).

454

455   **HDAC3 inhibition restores MHC class II expression in human DLBCL cell lines and**

456   **patient specimens.**

457   The frequency of MHC class II loss in DLBCL exceeds the frequency of *CREBBP*

458   mutations in this disease[13,21], through unknown mechanisms. The ability of HDAC3

459   inhibition to induce MHC class II expression in *CREBBP* WT DLBCL cells may therefore

460   have potentially broad implications for immunotherapy. Using RNA-sequencing data from

461   WT (OCI-Ly1) and mutant (OCI-Ly19 and OZ) DLBCL cell lines (**Figure 6A; Tables S11**

462   **and S12**) and qPCR analysis of PDX tumors treated *in vivo* (**Figure S14A-D**), we

463   confirmed that gene expression induced by HDAC3 inhibition was largely conserved in

464   both contexts. The expression of *PD-L1* was significantly higher in 4/4 PDX tumors

465   treated with 25mg/kg BRD3308 *in vivo* compared to vehicle control treated tumors, and

466   MHC class II expression was significantly higher in 3/4 PDX tumors (**Figure S14A-D**). We

467   extended upon this using immunohistochemical staining for MHC class II in tumors from

468   a *CREBBP R1446C* mutant PDX model (DFBL; **Figure 6B**) and a *CREBBP* wild-type

469   PDX model that was MHC class II negative at baseline (DR-NY2, **Figure 6C**). In tumors

470   from both models, *in vivo* treatment with BRD3308 led to a marked induction of MHC

471   class II expression. In a broader panel of *CREBBP* WT and mutant cell lines, we observed

472   that a core set of genes including *HLA-DR*, *CIITA* and *PD-L1* had consistently higher

473   expression in BRD3308-treated cells compared to the matched control, but with a higher

474   magnitude of induction in *CREBBP* mutant cell lines (**Figure 6D**). This trend was also

475   observed by flow cytometry for MHC class II, which extends upon our observations in

476   CRISPR/Cas9-modified cells by showing a reproducible increase in expression in a larger

477   panel of DLBCL cell lines, and a higher magnitude of induction in *CREBBP* mutant cell

478   lines (**Figure 6E**). Together, these results show that selective inhibition of HDAC3 using

479   BRD3308 can promote the expression of IFN and antigen presentation pathway genes in

480   both the *CREBBP* WT and mutant settings. However, the magnitude of induction is

481   greatest in *CREBBP* mutant cells owing, in part, to the preferential induction of IRF1

482   activity in these cells.

483

484   **HDAC3 inhibition drives T-cell activation and immune responses.**

485   Interferon signaling and antigen presentation are central to anti-tumor immune responses.

486   We therefore investigated whether HDAC3 inhibition could promote antigen-dependent

487   anti-tumor immunity. To test this, we implanted OCI-Ly18 DLBCL cells into NSG mice

488   and once tumors formed we injected human peripheral blood mononuclear cells (PBMCs)

489   including T-cells to expose them to antigens presented by the tumor cells. These are

490   likely to be histocompatibility antigens rather than tumor neoantigens, but are nonetheless

491   presented and recognized through MHC:TCR interactions. After *in vivo* priming, tumor

492   infiltrating lymphocytes (TILs) were co-cultured *in vitro* with OCI-Ly18 cells that were pre-

493   treated for 72h with increasing concentrations of BRD3308 to assess the effects on T-cell

494   activation and tumor cell killing (**Figure 7A**). The DLBCL cells that were epigenetically

495   primed for antigen presentation by BRD3308 significantly increased the activation of CD4

496   T-cells, as determined by CD69 expression (p<0.05; **Figure 7B**). As in prior experiments,

497 we observed cell-intrinsic effects of BRD3308 on OCI-Ly18 cells in the absence of TILs,

498 resulting in declining cell viability with higher concentrations of the inhibitor. However, the

499 effects of BRD3308 were markedly and significantly increased in the presence of TILs,

500 consistent with T-cell-directed killing of the tumor cells (P<0.001; **Figure 7C**). To confirm

501 that this killing was dependent on MHC:TCR interactions we also performed this

502 experiment in the presence of blocking antibodies for MHC class I, MHC class II or both.

503 Blocking one or the other of MHC class I or II rescued some of the cytotoxicity observed

504 in this assay, but blocking both MHC class I and class II together completely abrogated

505 the TIL-associated effect (**Figure 7C**). These data show that HDAC3 inhibition can

506 potentiate anti-tumor immune responses that are likely to be antigen-dependent because

507 they are driven by MHC:TCR interactions. Our identification of the interferon signaling

508 pathway, and IFN-γ itself, as a central component of the response to HDAC3 inhibition

509 led us to test whether IFN-γ levels may rise as a result of treatment. An ELISPOT analysis

510 of the IFN-γ levels from the TIL and OCI-Ly18 co-culture experiment revealed a striking

511 and significant increase in IFN-γ levels, even at the lowest concentrations of HDAC3

512 inhibitor (**Figure 7D and S15**).

513

514 Considering the manner in which to best harness the anti-lymphoma immunity effect of

515 HDAC3 inhibitors, we noted that induction of MHC class II is mechanistically linked to

516 IFN-γ associated PD-L1 upregulation, which could potentially limit maximal anti-tumor

517 response. We therefore posited that PD-1/PD-L1 blockade may be an attractive

518 combination regimen. To test this hypothesis we used a murine lymphoma

519 transplantation model in which splenocytes from *IµBcl6;Ezh2^{Y641F}* mice[5] were

520　transplanted into irradiated syngeneic wild-type recipients (**Figure 7E**). Aggressive

521　tumors formed within these mice, which we treated with either vehicle control, BRD3308

522　alone, αPD-L1 alone, or a BRD3308 + αPD-L1 combination. Treatment with BRD3308

523　led to a significant increase in serum IFN-γ within these mice, which was also observed

524　with αPD-L1 treatment and was even further enhanced in an additive manner by the

525　combination treatment (**Figure 7F**). Immunofluorescent staining for CD4 and CD8

526　showed significantly increased infiltration within the spleens from BRD3308-treated mice,

527　which was further increased by the combination therapy (**Figure 7G-J**). The ability of

528　BRD3308 and αPD-L1 combination to increase TILs was likely linked with the IFN-γ-

529　mediated PD-L1 induction that was observed in BRD3308-treated tumors (**Figure 7K-L**).

530　In line with this interaction, BRD3308 and αPD-L1 each showed a small degree of single-

531　agent efficacy, but the combination led to the most significant reduction in B220 cells

532　within the spleens of tumor-bearing mice (**Figure 7M-N**). Together these data show that

533　HDAC3 inhibitor-mediated reversal of the BCL6 repressed IFN pathway leads to joint

534　induction of MHC class II and PD-L1, which although eliciting significant anti-tumor

535　immune response, can be further enhanced by combination with PD-1/PD-L1 blockade

536　to yield a more potent immunotherapy strategy that is superior to checkpoint inhibition

537　alone.

538

539　**DISCUSSION**

540　Precision medicine and immunotherapy have led to significant breakthroughs in a variety

541　of cancers, but have lacked success in B-cell lymphoma. For precision medicine, this is

542　largely due to a paucity of 'actionable' genetic alterations or, rather, the lack of current

543   therapeutic avenues to target the mutations that have been defined as being important

544   for disease biology. For immunotherapy, the mechanisms driving lack of response or

545   early progression are not well understood, but are likely to be underpinned by the complex

546   immune microenvironment and genetic alterations that drive immune escape.   The

547   exception to both of these statements is the use of PD-1 neutralizing antibodies in

548   classical Hodgkin lymphoma, which opposes genetically-driven immune suppression by

549   the malignant Reed-Sternberg cells through DNA copy number gain of the PD-L1 locus[34]

550   and elicits responses in the majority of patients[35]. This stands as an example of the

551   potential success that could be achieved by the characterization and rational therapeutic

552   targeting of genetic alterations and/or the neutralization of immune escape mechanisms.

553   However, we are not yet able to successfully target some of the most frequently mutated

554   genes or overcome the barriers of inadequate response to immunotherapy in the most

555   common subtypes of B-cell lymphoma. These are important areas of need if we hope to

556   further improve the outcomes of these patients.

557

558   The *CREBBP* gene is mutated in ~15% of DLBCL[21] and ~66% of FL[7], and is therefore a

559   potentially high-yield target for precision therapeutic approaches. Our use of

560   CRISPR/Cas9 gene-editing to generate isogenic lymphoma cell lines that differ only in

561   their *CREBBP* mutation status allowed us to perform detailed characterization of the

562   epigenetic and transcriptional consequences of these mutations. Using this approach we

563   identified for the first time functional differences between the most frequent KAT domain

564   point mutation, R1446C, and frameshift mutations that result in KO. Although similar

565   regions of the genome showed reduced H3K27Ac in R1446C and KO mutants compared

566   to isogenic WT controls, the magnitude of these changes were markedly reduced in

567   *CREBBP* KO. This suggests that acetyltransferases such as EP300 may compensate for

568   the loss of CREBBP protein in the setting of *CREBBP* nonsense/frameshift mutations,

569   consistent with observations of functional redundancy between *Crebbp* and *Ep300* in B-

570   cell specific conditional knock-out mice[25,36]. But the presence of a catalytically inactive

571   CREBBP^{R1446C} protein may dominantly suppress histone acetylation by preventing the

572   participation of redundant acetyltransferases such as EP300 in transcriptional activating

573   complexes. This yields a more severe epigenetic and transcriptional phenotype in

574   *CREBBP^{R1446C}* mutants compared to *CREBBP^{KO}*, and an inferior clinical outcome.

575

576   Despite differences in the magnitude of molecular changes between R1446C and KO

577   cells, these mutations yielded a similar degree of synthetic vulnerability to HDAC3

578   inhibition. This was likely driven by the increased suppression of BCL6 target genes that

579   we observed in both contexts, including *CDKN1A* (p21). This gene has also been

580   highlighted as a critical nexus in the oncogenic potential of *EZH2*[37], which cooperates

581   with BCL6 to silence gene expression[5]. One of the important mechanisms for BCL6-

582   mediated gene silencing is through the recruitment of HDAC3 as part of the NCOR/SMRT

583   complex[3], thereby highlighting HDAC3 inhibition as a rational therapeutic avenue for

584   counteracting BCL6 activity. Virtually all of the HDAC3 corepressor complexes present

585   in DLBCL cells are bound with BCL6, suggesting that HDAC3 inhibitors effect is largely

586   explained by their depression of the subset of BCL6 target genes regulated through this

587   mechanism[3]. Importantly, as a variety of GCB-derived malignancies rely on BCL6

588   function independently of *CREBBP* or *EZH2* mutation[38,39], opposing this function through

589   HDAC3 inhibition may also be effective in tumors without these genetic alterations. We

590   have shown preliminary evidence in the primary setting using DLBCL PDX models.

591

592   One of the important transcriptional programs that is regulated by BCL6 is the interferon

593   signaling pathway[3], which we observed to be significantly repressed in *CREBBP* mutant

594   cells. It has been also long been recognized that IFN-γ cooperates with lymphocytes to

595   prevent cancer development[40]. Interferon signaling supports T-cell driven anti-tumor

596   immunity via a variety of mechanisms, including the induction of antigen presentation on

597   MHC class II[41], and the expression of MHC class II-restricted tumor antigens is required

598   for the spontaneous or immunotherapy-induced rejection of tumors[14]. We have shown

599   that the selective inhibition of HDAC3 is sufficient for broadly restoring the reduced

600   H3K27Ac and gene expression that is associated with *CREBBP* mutation, including the

601   interferon signaling and antigen presentation programs. This was in part driven by the

602   increased production of IFN-γ following HDAC3 inhibition, but also via the induced

603   expression and activity of the IRF1 transcription factor. Together, these factors lead to a

604   robust restoration of MHC class II expression on *CREBBP* mutant cells and drove dose-

605   dependent potentiation of anti-tumor T-cell responses. However, we also noted that the

606   same molecular signature is promoted by HDAC3 inhibition in *CREBBP* wild-type cells,

607   also with an associated increase of MHC class II expression. As with the cell-intrinsic

608   effects of HDAC3 inhibition, the effects on immune interactions may therefore be active

609   in both *CREBBP* wild-type and *CREBBP* mutant cells as a result of the conserved

610   molecular circuitry controlling these pathways in each genetic context.

611

612   A variety of HDAC inhibitors were capable of restoring antigen presentation in our models

613   and clinical responses are observed with these agents in relapsed/refractory FL and

614   DLBCL patients. However, grade 3-4 hematological toxicities such as thrombocytopenia,

615   anemia and neutropenia were frequent, and the responses tended not to be durable[42,43].

616   We posit that specific inhibition of HDAC3 may be accompanied by reduced toxicity, as

617   HDAC1 and HDAC2 have important roles in hematopoiesis[33] and avoiding the inhibition

618   of these HDACs may therefore avoid the undesired hematological effects associated with

619   pan-HDAC inhibition. In line with this, we observed that BRD3308 was less toxic to CD4

620   and CD8 T-cells than pan-HDAC inhibitors, and was able to elicit MHC-dependent T-cell

621   responses against a *CREBBP* wild-type DLBCL cell line *in vitro*. Although these

622   responses are likely driven by histocompatibility antigens rather than tumor neoantigens,

623   it supports the premise that selective HDAC3 inhibition is capable of promoting antigen

624   presentation and immune responses. We also speculate that the clinically-observed lack

625   of durability for HDAC inhibitors may be the result of adaptive immune suppression

626   through mechanisms such as PD-L1 induction, which dampens T-cell responses through

627   the PD-1 receptor[44], as well as direct toxicity of pan-HDAC inhibitors to T-cells. We found

628   evidence for adaptive immune suppression within our model systems, showing that

629   HDAC3 inhibition leads to increased IFN-γ production and the upregulation of *PD-L1*

630   expression. This is in line with recent observations that PD-L1 (*CD274*) is a BCL6-

631   supressed gene[45], and a well-characterized role for PD-L1 as an IFN-γ-responsive

632   gene[44].   In other cancers in which a florid antigen-driven immune response and

633   concomitant adaptive immune suppression via PD-L1 exist within the tumor

634   microenvironment, blockade of the PD-1 receptor is an effective therapeutic strategy[15,17].

635   Recent studies have also shown that the efficacy of PD-1 blockade is inextricably linked

636   with the existence of an interferon-driven immune response and expression of MHC class

637   II[15,17]. We have shown some evidence for this in a syngeneic, BCL6 driven murine model

638   of B-cell lymphoma, wherein the combination of HDAC3 inhibition and αPD-L1 led to

639   enhanced levels of CD4 and CD8 T-cell infiltration and clearance of tumor cells.

640   Together, these observations suggest that the greatest potentiation of anti-tumor

641   immunity in GCB-derived malignancies may be achieved through stimulation of interferon

642   signaling and MHC class II expression by HDAC3 inhibition, in combination with the

643   blockade of adaptive immune suppression using PD-L1/PD-1 neutralizing antibodies.

644   However, this concept requires further exploration in future studies.

645

646   In conclusion, this work defines a molecular circuit that controls the survival and

647   differentiation of lymphoma B-cells and their interaction with T-cells. This circuit is

648   antagonistically regulated by CREBBP and BCL6, and can be pushed towards promoting

649   tumor cell death and anti-tumor immunity via selective inhibition of HDAC3. This highlights

650   HDAC3 inhibition as an attractive therapeutic avenue, which may be broadly active in FL

651   and DLBCL due to the near-ubiquitous role of BCL6, but which may have enhanced

652   potency in *CREBBP* mutant tumors.

653

654

655

656

657

658   **MATERIALS AND METHODS**

659

660   For detailed methodology, please refer to the supplementary methods section.

661

662   CRISPR/Cas9-modification of lymphoma cells

663   The RL cell-line (ATCC CRL-2261) was modified by electroporation of one of two unique

664   gRNA sequences in the pSpCas9(BB)-2A-GFP vector (Addgene plasmid #48138, gift

665   from Feng Zhang)[46] with a single-stranded oligonucleotide donor template. Single GFP-

666   positive cells were sorted 3-4 days after transfection, colonies expanded and evaluated

667   for changes in the targeted region using Sanger sequencing. The process was repeated

668   for until point mutants were retrieved from each of the two gRNAs, totaling 742 single

669   clones. Potential off-target sites of each guide RNA were determined by BLAST, and all

670   sites with ≥16/20 nucleotide match to either of the gRNA sequences was interrogated by

671   Sanger sequencing (**Table S13**). All cells were maintained as sub-confluent culture in

672   RPMI medium with 10% FBS and PenStrep and re-validated by Sanger sequencing prior

673   to each set of experiments. Basic phenotyping of the cell lines is presented in **Figure**

674   **S16A-E**.

675

676   ChIP-sequencing

677   Cells were washed and fixed in formaldehyde, and chromatin sheared by sonication. An

678   antibody specific to H3K27Ac (Active Motif) was coupled to magnetic protein G beads,

679   incubated with chromatin overnight, and immunoprecipitation performed. Input controls

680   were reserved for comparison. Nucleosomal DNA was isolated and either used as a

681 template for qPCR (ChIP-qPCR) or to generate NGS libraries using KAPA Hyper Prep

682 Kits (Roche) and TruSeq adaptors (Bioo Scientific) using 6 cycles of PCR enrichment.

683 Libraries were 6-plexed and sequenced with 2x100bp reads on a HiSeq-4000 (Illumina).

684 The data were mapped using BWA, peaks called using MACS2, and differential analyses

685 performed using DiffBind. For gene set enrichment analyses, the gene with the closest

686 transcription start site to the peak was used. The statistical thresholds for significance

687 were $q<0.05$ and fold-change>1.5.

688

689 RNA-sequencing

690 Total RNA was isolated using AllPrep DNA/RNA kits (Qiagen) and evaluated for quality

691 on a Tapestation 4200 instrument (Agilent). Total RNA (1µg) was used for library

692 preparation with KAPA HyperPrep RNA kits with RiboErase (Roche) and TruSeq

693 adapters (Bioo Scientific). Libraries were validated on a Tapestation 4200 instrument

694 (Agilent), quantified by Qubit dsDNA kit (Life Technologies), 6-plexed, and sequenced on

695 a HiSeq4000 instrument at the MD Anderson Sequencing and Microarray Facility using

696 2x100bp reads. Reads were aligned with STAR, and differential gene expression analysis

697 performed with DEseq2. The statistical thresholds for significance were $q<0.05$ and fold-

698 change>2.

699

700 Cell proliferation assays

701 Cells were seeded in 96-well plates at 50,000 cell/100 µl/well with either vehicle (DMSO

702 0.1%) or increasing concentrations of drugs. Cell viability was assessed with the

703 fluorescent redox dye CellTiter-Blue (Promega). The reagent was added to the culture

704   medium at 1:5 dilution, according to manufacturer`s instructions. Procedures to determine

705   the effects of certain conditions on cell proliferation and apoptosis were performed in 3

706   independent experiments. The 2-tailed Student t test and Wilcoxon Rank test were used

707   to estimate the statistical significance of differences among results from the 3

708   experiments. Significance was set at $P < .05$. The PRISM software was used for the

709   statistical analyses.

710

711   <u>Patient-derived xenograft and in vitro organoid studies.</u>

712   A *CREBBP* R1446C mutant tumor (DFBL13727) was obtained from the public repository

713   of xenografts[47], expanded for 12 weeks in 1 mouse by surgical implantation into the renal

714   capsule, then implanted into the renal capsule 12 additional mice for efficacy studies.

715   Tumors were allowed to grow for 6 weeks, the size measured by MRI and mice

716   randomized to treatment and control groups to similar average tumor sizes. Mice were

717   treated with BRD3308 (25mg/kg) or vehicle control twice per day, 5 days on and 2 days

718   off for a total of 3 weeks, and tumor size assessed by MRI every 7 days. Two mice per

719   group were euthanized on day 10 and the tumors harvested for biomarker analysis. Mice

720   were cared for in accordance with guidelines approved by the MD Anderson Institutional

721   Animal Care and Use Committee.

722

723   For *CREBBP* wild-type tumors (NY-DR2, DANA and TONY), six week old female NSG

724   mice were implanted subcutaneously and treatments started when tumors reached 100

725   mm3. Mice (12/group) were randomized and dosed via oral gavage with BRD3308 (25

726   mg/kg) or control vehicle (0.5% methyl cellulose, 0.2% tween 80) twice daily for 21

727   consecutive days. Mice were cared for in accordance with guidelines approved by the

728   Memorial Sloan Kettering Cancer Center Institutional Animal Care and Use Committee

729   and Research Animal Resource Center.

730

731   For *in vitro* organoid culture, the tumors were dissociated to single cells, stained with

732   CFSE, washed and mixed with irradiated 40LB cells at a 10:1 ratio of Primary:40LB. The

733   cell mixture was then used to fabricate organoids in a 96-well plate as previously

734   described[48], with 20 μL organoids containing 3% silicate nanoparticles and a 5% gelatin

735   in IMDM medium solution. The organoids were cultured in IMDM medium containing 20%

736   FBS supplemented with antibiotics and normocin (Invivogen) for 6 days, doubling the

737   volume of medium after 3 days. The cell mixture was exposed to 4 1:3 serial dilutions of

738   BRD3308 starting at 5 μM or vehicle control (DMSO) in triplicate for 6 days, treating a

739   second time at 3 days. After 6 days of exposure, cell viability and proliferation were

740   assessed by flow cytometry using DAPI staining gating on CFSE-positive cells.

741

742   <u>Ex vivo killing assay.</u> The OCI-LY18 was subcutaneously implanted in NSG mice and

743   allowed to become established before the mice were injected with PBMC. After 2 weeks,

744   the tumors were dissociated to single cells and CD3+ TILs were positively selected. T

745   cells were expanded with a single administration of immunomagnetic microbeads coated

746   with mouse anti-human CD3 and CD28 mAb, rhIL2 and rhIL15 for 5 days. OCI-LY18 cells

747   were treated with either DMSO or 10μM BRD3308 for 3 days, washed and resuspended

748   in fresh media with or without T cells at a ratio of 1:10. For MHC blocking, OCI-LY18 cells

749   treated with 10μg/mL of either isotype Ig, or blocking Ab against HLA-ABC W6/32, HLA-

750   DR/DP/DQ or the combination of the two. After 24 hours co-culture, cell viability was

751   analyzed using CellTiter Blue.

752

753   <u>Immunocompetent *IµBcl6;Ezh2^{Y641F}* model.</u> 6 weeks old female C56BL/6J mice were

754   irradiated at day -1 and 0 with 250 rad, and after 2 hours transplanted with 1 x 10^6

755   splenocytes from *IµBcl6;Ezh2^{Y641F}* mice[5] and 0.2 x 10^6 bone marrow cells from a healthy

756   age-matched donor. Three weeks after transplantation, mice became sick and treatment

757   was initiated with either vehicle or BRD3308 (25 mg/kg twice daily, every day for 21 days)

758   via oral gavage, with or without αPDL1 antibody delivered by intraperitoneal injection (250

759   µg twice weekly for 4 administration). Mice were monitored daily and euthanized when

760   they became moribund. Spleen and liver where measured, weighed and analyzed by flow

761   cytometry for evaluating the disease. Immunofluorescent staining and imaging were

762   performed at the Molecular Cytology Core Facility of Memorial Sloan Kettering Cancer

763   Center. Sections were stained with either anti- CD4 (R&D Systems, cat#AF554, 2ug/ml)

764   or anti-PD-L1 (R&D Systems cat#AF1019, 2ug/ml) or B220 (BD Biosciences, cat#

765   550286, 0.3ug/ml) or anti-CD8 (eBiosciences cat# 14-0808, 2.5ug/ml) for 5 hours,

766   followed by 60 minutes incubation with biotinylated horse anti-goat IgG (forCD4 and PD-

767   L1) (Vector cat#BA-9500) or biotinylated goat anti-rat IgG (for CD8 and B220) (Vector

768   labs, cat#BA9400) at 1:200 dilution. The detection was performed with Streptavidin-HRP

769   D (part of DABMap kit, Ventana Medical Systems), followed by incubation with Tyramide

770   Alexa 488 (Invitrogen, cat# B40953), and counterstaining with DAPI (Sigma Aldrich, cat#

771   D9542, 5 ug/ml). The slides were scanned with a Pannoramic Flash P250 Scanner

772   (3DHistech,Hungary) using a 20x/0.8NA objective lens. The fluorescence channels were

773   imaged using DAPI, FITC, and TRITC filters sequentially with manually adjusted

774   exposure times. Images were then exported into .tifs using Caseviewer

775   (3DHistech,Hungary) to be analyzed.

776

777   **DATA DEPOSITION**

778   The RNA-seq and ChIP-seq data are available at the Gene Expression Omnibus

779   database under accession number GSE142357.

780

781   **ACKNOWLEDGEMENTS**

789

790

791

792

793

794

795

REFERENCES

1   Hatzi, K. & Melnick, A. Breaking bad in the germinal center: how deregulation of BCL6 contributes to lymphomagenesis. *Trends Mol Med* **20**, 343-352, doi:10.1016/j.molmed.2014.03.001 (2014).

2   Mesin, L., Ersching, J. & Victora, G. D. Germinal Center B Cell Dynamics. *Immunity* **45**, 471-482, doi:10.1016/j.immuni.2016.09.001 (2016).

3   Hatzi, K. *et al.* A hybrid mechanism of action for BCL6 in B cells defined by formation of functionally distinct complexes at enhancers and promoters. *Cell reports* **4**, 578-588, doi:10.1016/j.celrep.2013.06.016 (2013).

4   Hatzi, K. *et al.* Histone demethylase LSD1 is required for germinal center formation and BCL6-driven lymphomagenesis. *Nature immunology* **20**, 86-96, doi:10.1038/s41590-018-0273-1 (2019).

5   Beguelin, W. *et al.* EZH2 and BCL6 Cooperate to Assemble CBX8-BCOR Complex to Repress Bivalent Promoters, Mediate Germinal Center Formation and Lymphomagenesis. *Cancer cell* **30**, 197-213, doi:10.1016/j.ccell.2016.07.006 (2016).

6   Green, M. R. Chromatin modifying gene mutations in follicular lymphoma. *Blood* **131**, 595-604, doi:10.1182/blood-2017-08-737361 (2018).

7   Green, M. R. *et al.* Mutations in early follicular lymphoma progenitors are associated with suppressed antigen presentation. *Proceedings of the National Academy of Sciences of the United States of America* **112**, E1116-1125, doi:10.1073/pnas.1501199112 (2015).

8   Jiang, Y. *et al.* CREBBP Inactivation Promotes the Development of HDAC3-Dependent Lymphomas. *Cancer discovery* **7**, 38-53, doi:10.1158/2159-8290.CD-16-0975 (2017).

9   Allen, C. D., Okada, T. & Cyster, J. G. Germinal-center organization and cellular dynamics. *Immunity* **27**, 190-202, doi:10.1016/j.immuni.2007.07.009 (2007).

10   Khodadoust, M. S. *et al.* Antigen presentation profiling reveals recognition of lymphoma immunoglobulin neoantigens. *Nature* **543**, 723-727, doi:10.1038/nature21433 (2017).

11   Khodadoust, M. S. *et al.* B cell lymphomas present immunoglobulin neoantigens. *Blood* **133**, 878-881, doi:10.1182/blood-2018-06-845156 (2018).

12   Marty, R., Thompson, W. K., Salem, R. M., Zanetti, M. & Carter, H. Evolutionary Pressure against MHC Class II Binding Cancer Mutations. *Cell* **175**, 416-428, doi:10.1016/j.cell.2018.08.048 (2018).

13   Rimsza, L. M. *et al.* Loss of MHC class II gene and protein expression in diffuse large B-cell lymphoma is related to decreased tumor immunosurveillance and poor patient survival regardless of other prognostic factors: a follow-up study from the Leukemia and Lymphoma Molecular Profiling Project. *Blood* **103**, 4251-4258, doi:10.1182/blood-2003-07-2365 (2004).

14   Alspach, E. *et al.* MHC-II neoantigens shape tumour immunity and response to immunotherapy. *Nature* **574**, 696-701, doi:10.1038/s41586-019-1671-8 (2019).

15   Rodig, S. J. *et al.* MHC proteins confer differential sensitivity to CTLA-4 and PD-1 blockade in untreated metastatic melanoma. *Science translational medicine* **10**, eaar3342, doi:10.1126/scitranslmed.aar3342 (2018).

16   Ayers, M. *et al.* IFN-gamma-related mRNA profile predicts clinical response to PD-1 blockade. *The Journal of clinical investigation* **127**, 2930-2940, doi:10.1172/JCI91190 (2017).

17   Tumeh, P. C. *et al.* PD-1 blockade induces responses by inhibiting adaptive immune resistance. *Nature* **515**, 568-571, doi:10.1038/nature13954 (2014).

18   Borst, J., Ahrends, T., Babala, N., Melief, C. J. M. & Kastenmuller, W. CD4(+) T cell help in cancer immunology and immunotherapy. *Nature reviews. Immunology* **18**, 635-647, doi:10.1038/s41577-018-0044-0 (2018).

845 19   Garcia-Ramirez, I. *et al.* Crebbp loss cooperates with Bcl2 over-expression to promote
846   lymphoma in mice. *Blood* **129**, 2645-2656, doi:10.1182/blood-2016-08-733469 (2017).
847 20   Mullighan, C. G. *et al.* CREBBP mutations in relapsed acute lymphoblastic leukaemia.
848   *Nature* **471**, 235-239, doi:10.1038/nature09727 (2011).
849 21   Pasqualucci, L. *et al.* Inactivating mutations of acetyltransferase genes in B-cell
850   lymphoma. *Nature* **471**, 189-195, doi:10.1038/nature09730 (2011).
851 22   Hashwah, H. *et al.* Inactivation of CREBBP expands the germinal center B cell
852   compartment, down-regulates MHCII expression and promotes DLBCL growth.
853   *Proceedings of the National Academy of Sciences of the United States of America*,
854   doi:10.1073/pnas.1619555114 (2017).
855 23   Horton, S. J. *et al.* Early loss of Crebbp confers malignant stem cell properties on
856   lymphoid progenitors. *Nat Cell Biol* **19**, 11093-11104, doi:10.1038/ncb3597 (2017).
857 24   Zhang, J. *et al.* The Crebbp Acetyltransferase is a Haploinsufficient Tumor Suppressor in
858   B Cell Lymphoma. *Cancer discovery* **7**, 322-337, doi:10.1158/2159-8290.CD-16-1417
859   (2017).
860 25   Meyer, S. N. *et al.* Unique and Shared Epigenetic Programs of the CREBBP and EP300
861   Acetyltransferases in Germinal Center B Cells Reveal Targetable Dependencies in
862   Lymphoma. *Immunity* **51**, 535-547, doi:10.1016/j.immuni.2019.08.006 (2019).
863 26   Pastore, A. *et al.* Integration of gene mutations in risk prognostication for patients
864   receiving first-line immunochemotherapy for follicular lymphoma: a retrospective analysis
865   of a prospective clinical trial and validation in a population-based registry. *Lancet Oncol*
866   **16**, 1111-1122, doi:10.1016/S1470-2045(15)00169-2 (2015).
867 27   Li, J. *et al.* Both corepressor proteins SMRT and N-CoR exist in large protein complexes
868   containing HDAC3. *EMBO J* **19**, 4342-4350, doi:10.1093/emboj/19.16.4342 (2000).
869 28   Wagner, F. F. *et al.* An Isochemogenic Set of Inhibitors To Define the Therapeutic
870   Potential of Histone Deacetylases in beta-Cell Protection. *ACS Chem Biol* **11**, 363-374,
871   doi:10.1021/acschembio.5b00640 (2016).
872 29   Phan, R. T., Saito, M., Basso, K., Niu, H. & Dalla-Favera, R. BCL6 interacts with the
873   transcription factor Miz-1 to suppress the cyclin-dependent kinase inhibitor p21 and cell
874   cycle arrest in germinal center B cells. *Nature immunology* **6**, 1054-1060,
875   doi:10.1038/ni1245 (2005).
876 30   Tian, Y. F. *et al.* Integrin-specific hydrogels as adaptable tumor organoids for malignant
877   B and T cells. *Biomaterials* **73**, 110-119, doi:10.1016/j.biomaterials.2015.09.007 (2015).
878 31   Fujita, N. *et al.* MTA3 and the Mi-2/NuRD complex regulate cell fate during B lymphocyte
879   differentiation. *Cell* **119**, 75-86, doi:10.1016/j.cell.2004.09.014 (2004).
880 32   Huang, C. *et al.* The BCL6 RD2 domain governs commitment of activated B cells to form
881   germinal centers. *Cell reports* **8**, 1497-1508, doi:10.1016/j.celrep.2014.07.059 (2014).
882 33   Wilting, R. H. *et al.* Overlapping functions of Hdac1 and Hdac2 in cell cycle regulation
883   and haematopoiesis. *EMBO J* **29**, 2586-2597, doi:10.1038/emboj.2010.136 (2010).
884 34   Green, M. R. *et al.* Integrative analysis reveals selective 9p24.1 amplification, increased
885   PD-1 ligand expression, and further induction via JAK2 in nodular sclerosing Hodgkin
886   lymphoma and primary mediastinal large B-cell lymphoma. *Blood* **116**, 3268-3277,
887   doi:10.1182/blood-2010-05-282780 (2010).
888 35   Ansell, S. M. *et al.* PD-1 blockade with nivolumab in relapsed or refractory Hodgkin's
889   lymphoma. *The New England journal of medicine* **372**, 311-319,
890   doi:10.1056/NEJMoa1411087 (2015).
891 36   Xu, W. *et al.* Global transcriptional coactivators CREB-binding protein and p300 are
892   highly essential collectively but not individually in peripheral B cells. *Blood* **107**, 4407-
893   4416, doi:10.1182/blood-2005-08-3263 (2006).

894 37 Beguelin, W. *et al.* EZH2 enables germinal centre formation through epigenetic silencing
895   of CDKN1A and an Rb-E2F1 feedback loop. *Nature communications* **8**, 877,
896   doi:10.1038/s41467-017-01029-x (2017).
897 38 Valls, E. *et al.* BCL6 Antagonizes NOTCH2 to Maintain Survival of Human Follicular
898   Lymphoma Cells. *Cancer discovery* **7**, 506-521, doi:10.1158/2159-8290.CD-16-1189
899   (2017).
900 39 Cardenas, M. G. *et al.* Rationally designed BCL6 inhibitors target activated B cell diffuse
901   large B cell lymphoma. *The Journal of clinical investigation* **126**, 3351-3362,
902   doi:10.1172/JCI85795 (2016).
903 40 Shankaran, V. *et al.* IFNgamma and lymphocytes prevent primary tumour development
904   and shape tumour immunogenicity. *Nature* **410**, 1107-1111, doi:10.1038/35074122
905   (2001).
906 41 Minn, A. J. & Wherry, E. J. Combination Cancer Therapies with Immune Checkpoint
907   Blockade: Convergence on Interferon Signaling. *Cell* **165**, 272-275,
908   doi:10.1016/j.cell.2016.03.031 (2016).
909 42 Ogura, M. *et al.* A multicentre phase II study of vorinostat in patients with relapsed or
910   refractory indolent B-cell non-Hodgkin lymphoma and mantle cell lymphoma. *British
911   journal of haematology* **165**, 768-776, doi:10.1111/bjh.12819 (2014).
912 43 Crump, M. *et al.* Phase II trial of oral vorinostat (suberoylanilide hydroxamic acid) in
913   relapsed diffuse large-B-cell lymphoma. *Annals of oncology : official journal of the
914   European Society for Medical Oncology / ESMO* **19**, 964-969,
915   doi:10.1093/annonc/mdn031 (2008).
916 44 Zaidi, M. R. & Merlino, G. The two faces of interferon-gamma in cancer. *Clinical cancer
917   research : an official journal of the American Association for Cancer Research* **17**, 6118-
918   6124, doi:10.1158/1078-0432.CCR-11-0482 (2011).
919 45 Peng, C. *et al.* BCL6-Mediated Silencing of PD-1 Ligands in Germinal Center B Cells
920   Maintains Follicular T Cell Population. *Journal of immunology* **202**, 704-713,
921   doi:10.4049/jimmunol.1800876 (2018).
922 46 Ran, F. A. *et al.* Genome engineering using the CRISPR-Cas9 system. *Nature protocols*
923   **8**, 2281-2308, doi:10.1038/nprot.2013.143 (2013).
924 47 Townsend, E. C. *et al.* The Public Repository of Xenografts Enables Discovery and
925   Randomized Phase II-like Trials in Mice. *Cancer cell* **29**, 574-586,
926   doi:10.1016/j.ccell.2016.03.008 (2016).
927 48 Purwada, A. *et al.* Ex vivo engineered immune organoids for controlled germinal center
928   reactions. *Biomaterials* **63**, 24-34, doi:10.1016/j.biomaterials.2015.06.002 (2015).

929

930

931

932

933

934

935

936

Figure 1: Detailed molecular characterization of CREBBP^{R1446C} and CREBBP^{KO} mutations using isogenic CRISPR/Cas9-modified lymphoma cells. A) A diagram shows the CRISPR/Cas9 gene editing strategy. Two guides were designed that were proximal to the R1446 codon, with PAM sites highlighted in yellow. A single stranded Homologous Recombination (HR) template was utilized that encoded silent single nucleotide changes that interfered with the PAM sites but did not change the protein coding sequence, and an additional single nucleotide change that encoded the R1446C mutation. **B)** A representative western blot shows that the CREBBP^{R1446C} protein is expressed at similar levels to that of wild-type CREBBP, whereas CREBBP^{KO} results in a complete loss of protein expression as expected. The level of H3K27Ac shows a more visible reduction in *CREBBP^{R1446C}* cells compared to isogenic *CREBBP^{WT}* cells than that observed in *CREBBP^{KO}* cells. **C)** Quantification of triplicate western blot experiments shows that there is a significant reduction of H3K27Ac in *CREBBP^{R1446C}* cells compared to *CREBBP^{WT}* cells (T-test p-value <0.001). A reduction is also observed in *CREBBP^{KO}* cells, but this was not statistically significant (T-test p-value = 0.106). **D)** Heat maps show the regions of significant H3K27Ac loss (n=2022, above) and gain (n=2304, below) in *CREBBP^{R1446C}* cells compared to isogenic WT controls. The regions with reduced H3K27Ac in *CREBBP^{R1446C}* cells can be seen to normally bear this mark in GCB cells. **E)** Density plots show that the degree of H3K27Ac loss (above) is most notable in *CREBBP^{R1446C}* cells compared to isogenic WT cells, while *CREBBP^{KO}* cells show an intermediate level of loss. Regions with H3K27Ac gain (below) in *CREBBP^{R1446C}* cells showed fewer changes in *CREBBP^{KO}* cells. **F)** A heat map of RNA-seq data shows that there are a similar number of genes with increased (n=766) and decreased (n=733) expression in *CREBBP^{R1446C}* cells compared to isogenic WT controls. The *CREBBP^{KO}* cells again show an intermediate level of change, with expression between that of *CREBBP^{WT}* and *CREBBP^{R1446C}* cells. **G)** Gene set enrichment analysis of the genes most closely associated with regions of H3K27Ac gain (above) or loss (below) shows that these epigenetic changes are significantly associated with coordinately increased or decreased expression in *CREBBP^{R144C}* cells compared to isogenic WT controls, respectively. **H)** Gene set enrichment analysis shows that genes which were previously found to be down-regulated following shRNA-mediated knock-down of *CREBBP* in murine B-cells (top) or human lymphoma cell lines (middle) are also reduced in *CREBBP^{R1446C}* mutant cells compared to *CREBBP^{WT}* cells. However, the most significant enrichment was observed for the signature of genes that we found to be significantly reduced in primary human FL with *CREBBP* mutation compared to *CREBBP* wild-type tumors. **I)** Hypergeometric enrichment analysis identified sets of genes that were significantly over-represented in those with altered H3K27Ac or expression in *CREBBP^{R1446C}* cells. This included (i) gene sets associated with *CREBBP* mutation in primary tumors, (ii) BCL6 target genes, (iii) BCR and IL4 signaling pathways, and (iv) gene sets involving immune responses, antigen presentation and interferon signaling were significantly enriched. **J)** ChIP-seq tracks of the MHC class II locus on chromosome 6 are shown for isogenic *CREBBP^{WT}* (blue), *CREBBP^{R1446C}* (red) and *CREBBP^{KO}* (orange) cells with regions of significant H3K27Ac loss shaded in grey. A significant reduction can be observed between *CREBBP^{WT}* and *CREBBP^{R1446C}* cells, with *CREBBP^{KO}* cells harboring an intermediate level H3K27Ac over these loci. **K)** Flow cytometry for HLA-DR shows that reduced H3K27Ac over the MHC class II region is associated with changes of cell surface protein expression. A ~2-fold

983 reduction is observed in $CREBBP^{KO}$ cell compared to $CREBBP^{WT}$, but a dramatic ~39-
984 fold reduction is observed in $CREBBP^{R1446C}$ cells. **L)** Kaplan-Meier plots show the failure
985 free survival in 231 previously untreated FL patients according to their $CREBBP$ mutation
986 status. Nonsense/frameshift mutations that create a loss-of-protein (LOP) are associated
987 with a significantly better failure-free survival compared to KAT domain point mutations
988 (KAT P.M.; log-rank P=0.026). **M)** Kaplan-Meier plots show the overall survival in 231
989 previously untreated FL patients according to their $CREBBP$ mutation status. Patients
990 with LOP mutations have a trend towards better overall survival, but this is not statistically
991 significant (log-rank P=0.118).
992
993
994
995
996
997
998
999
1000
1001
1002
1003
1004
1005
1006
1007
1008
1009
1010
1011
1012
1013
1014
1015
1016
1017
1018
1019
1020
1021
1022
1023
1024
1025
1026
1027

Figure 2: Synthetic dependence upon BCL6 and HDAC3 in *CREBBP* mutant cells.
A) A heat map shows that regions with reduced H3K27Ac in *CREBBP^{R1446C}* cells compared to *CREBBP^{WT}* cells (above) are bound by both CREBBP and BCL6 in normal germinal center B-cells. This binding is not observed over regions with increased H3K27Ac in mutant cells. **B)** Isogenic *CREBBP^{R1446C}* and *CREBBP^{KO}* cells have a greater sensitivity to BRD3308, a selective HDAC3 inhibitor, compared to *CREBBP^{WT}* cells. **C)** Knock-down of HDAC3 with two unique shRNAs shows a similar preference towards limiting cell proliferation in *CREBBP^{R1446C}* cells compared to WT. Data are shown relative to control shRNA in the same cell lines (*P<0.05, ***P<0.001). **D)** Representative western blots show a dose-dependent increase in H3K27Ac in both *CREBBP^{WT}* and *CREBBP^{R1446C}* cells treated with BRD3308, compared to the control compound BRD4097. **E)** ChIP-seq tracks of H3K27Ac show that *CREBBP^{KO}* and *CREBBP^{R1446C}* both have reduced levels over the *CDKN1A* locus compared to isogenic *CREBBP^{WT}* cells. Regions that are statistically significant are shaded in grey. **F)** A representative western blot shows that CDKN1A is induced at the protein level by treatment with 10µM BRD3308 in both *CREBBP^{WT}* and *CREBBP^{R1446C}* cells. **G)** Knock-down of CDKN1A (p21) using two unique shRNAs partially rescued the proliferative arrest of cells treated with BRD3308. This rescue was more significant in *CREBBP* mutant cells compared to wild-type. Data are displayed relative to vehicle-treated cells (*P<0.05, **P<0.01, ***P<0.001). **H)** The difference in sensitivity to BRD3308 between *CREBBP* wild-type (blue) and *CREBBP* mutant (yellow to red) was validated in a large panel of DLBCL cell lines. **I)** The effective dose 50 (ED50) concentrations for each cell line from (H) are shown, colored by *CREBBP* mutation status. The ED50s for *CREBBP* mutant (red) cell lines was significantly lower than that observed for *CREBBP* wild-type cell lines (blue; T-test P=0.002). **J)** Gene set enrichment analysis of 'Germinal Center Terminal Differentiation' signature genes shows that these genes are coordinately induced in both *CREBBP* wild-type (above) and mutant (below) DLBCL cell lines by BRD3308 treatment compared to control.

Figure 3: BRD3308 is effective in primary DLBCL. A) The sensitivity of primary DLBCL tumors to BRD3308 was evaluated by expanding them *in vivo*, followed by culture in our *in vitro* organoid model with different concentrations of BRD3308. A dose-dependent decrease in cell viability was observed in all 6 tumors with increasing concentrations of BRD3308. **B)** Treatment of 3 unique DLBCL xenograft models *in vivo* with 25mg/kg (green) or 50mg/kg (orange) of BRD3308 significantly reduced tumor growth compared to vehicle (black) (**P<0.01; ***P<0.001). **C)** Representative MRI images of renal capsule implanted PDX tumors from a $CREBBP^{R1446C}$ mutant DLBCL at the beginning (day 0) and day 14 of treatment. Tumor is outlined in yellow. **D)** Quantification of tumor volume by MRI images, normalized to the pre-treatment volume for the same tumor, shows that BRD3308 treatment significantly reduces tumor growth (*P<0.05, **P<0.01).

1118 **Figure 4: HDAC3 inhibition counteracts the molecular phenotype of *CREBBP***
1119 ***mutation. A)*** A heat map shows the regions with significantly increased (above, n=6756)
1120 or decreased (below, n=1916) H3K27Ac in *CREBBP*^*R1446C*^ cells treated with BRD3308
1121 compared to those treated with the control compound, BRD4097. Experimental duplicates
1122 are shown for each clone. **B)** A river plot show that a large fraction of the regions with
1123 significantly reduced H3K27Ac in *CREBBP*^*R1446C*^ cells compared to *CREBBP*^*WT*^ cells had
1124 significantly increased H3K27Ac following BRD3308 treatment. **C)** A density plot shows
1125 the regions with reduced H3K27Ac in *CREBBP*^*R1446C*^ compared to *CREBBP*^*WT*^ cells. The
1126 level of H3K27Ac over these regions is increased in *CREBBP*^*R1446C*^ cells treated with
1127 BRD3308 compared to control (BRD4097), but does not reach the level observed in
1128 *CREBBP*^*WT*^ cells. **D)** A heat map shows the genes with increased (above, n=1467) or
1129 decreased expression (below, n=209) following BRD3308 treatment. Duplicate
1130 experiments are shown for each of the two *CREBBP*^*R1446C*^ clones. Interferon-responsive
1131 genes, including those with a role in antigen processing and presentation, can be
1132 observed to increase in expression following BRD3308 treatment. **E)** Gene set
1133 enrichment analysis shows that the set of genes with reduced H3K27Ac in association
1134 with *CREBBP* mutation has coordinately increased expression following BRD3308
1135 treatment. **F)** A density plot illustrates the relative change in promoter (red) and enhancer
1136 (blue) H3K27Ac following treatment with BRD3308, with the enhancer distribution being
1137 significantly more right-shifted (increased) compared to promoter regions. **G)** A heat map
1138 shows the change in H3K27Ac at the promoter regions of MHC class II genes following
1139 BRD3308 treatment of *CREBBP*^*R1446C*^ cells, showing a coordinate increase. **H-I)** Regions
1140 with significantly increased H3K27Ac (shaded in grey) included those within the MHC
1141 class II and *CIITA* gene loci. **J)** The increased expression of candidate genes within the
1142 interferon signaling and antigen presentation pathways was confirmed by qPCR.
1143 Increased expression was observed in both *CREBBP*^*WT*^ and *CREBBP*^*R1446C*^ cells
1144 following BRD3308 treatment, but the level of induction was much higher in
1145 *CREBBP*^*R1446C*^ cells. Data are shown relative to vehicle treated cells (T-test *P<0.05,
1146 **P<0.01, ***P<0.001). **K)** The on-target role of HDAC3 in the induction of candidate
1147 genes was confirmed by shRNA-mediated knock-down of HDAC3 and qPCR analysis of
1148 gene expression. Knock-down of HDAC3 was able to induce the expression of all genes,
1149 which is shown relative the control shRNA (T-test *P<0.05, **P<0.01, ***P<0.001).
1150
1151
1152
1153
1154
1155
1156
1157
1158
1159
1160
1161
1162
1163

1164 **Figure 5: HDAC3 inhibition induces interferon signaling and antigen presentation
1165 in both *CREBBP* wild-type and mutant cells. A)** Flow cytometry was performed for
1166 HLA-DR following exposure to a selection of HDAC inhibitors at 10μM for 72h. This shows
1167 that HDAC inhibitors with a range specificities are able to induce MHC class II, but HDAC3
1168 selective inhibition using BRD3308 is sufficient for this effect. **B)** Dose titrations of histone
1169 deacetylase inhibitors from (A) with peripheral blood CD4 and CD8 T-cells from healthy
1170 donors. **C)** A heat map of interferon responsive and antigen presentation genes from
1171 RNA-seq data shows an increased expression in both *CREBBP^WT^* and *CREBBP^R1446C^*
1172 cells. Data represent duplicate experiments for each clone and are normalized to control
1173 treated cells from the same experiment. **D)** Gene set enrichment analysis of the genes
1174 that have reduced H3K27Ac in *CREBBP^R1446C^* cells shows that the expression of these
1175 same genes are coordinately increased by BRD3308 treatment in *CREBBP^WT^* cells. **E)** A
1176 heat map of hypergeometric enrichment analysis results of RNA-seq data shows that
1177 BRD3308 induces the induction of similar gene sets in both *CREBBP^WT^* and
1178 *CREBBP^R1446C^* cells. **F)** A density strip plot, normalized to the mean expression in control
1179 (BRD4097)-treated *CREBBP^WT^* cells shows the relative expression of the set of genes
1180 with reduced H3K27Ac in *CREBBP^R1446C^* cells. This shows that these genes are induced
1181 by BRD3308 in *CREBBP^WT^* cells, resulting in expression levels greater than baseline.
1182 Further, *CREBBP^R1446C^* cells can be observed to start below baseline, with the induction
1183 by BRD3308 resulting in expression levels similar to that observed in control treated
1184 *CREBBP^WT^* cells. The 4 samples per condition represent duplicate experiments in each
1185 of the two clones for each genotype. **G)** The firefly luciferase luminescence of two unique
1186 IRF1 reporters (R1 and R2) is shown, normalized to renilla luciferase from a control vector
1187 and shown as fold change compared to untreated cells. *CREBBP^WT^* cells show increased
1188 IRF1 activity following IFN-γ treatment (positive control; grey), but not following treatment
1189 with BRD3308 (green). In contrast, *CREBBP^R1446C^* cells show increased IRF1 activity
1190 following BRD3308 treatment, to a level that is similar to that observed with IFN-γ
1191 treatment. (T-test vs control-treated cells, **P<0.01, ***P<0.001). **H)** The role of IFN-γ in
1192 inducing MHC class II expression following BRD3308 in *CREBBP^R1446C^* cells was
1193 assessed with a blocking experiment. Blocking IFN-γ with a neutralizing antibody (αIFN-
1194 γ) significantly reduced the induction of MHC class II, as measured by flow cytometry for
1195 HLA-DR, but the induction by BRD3308 with α IFN-γ remained significantly higher than
1196 vehicle with αIFN-γ (T-test, ***P<0.001).
1197
1198
1199
1200
1201
1202
1203
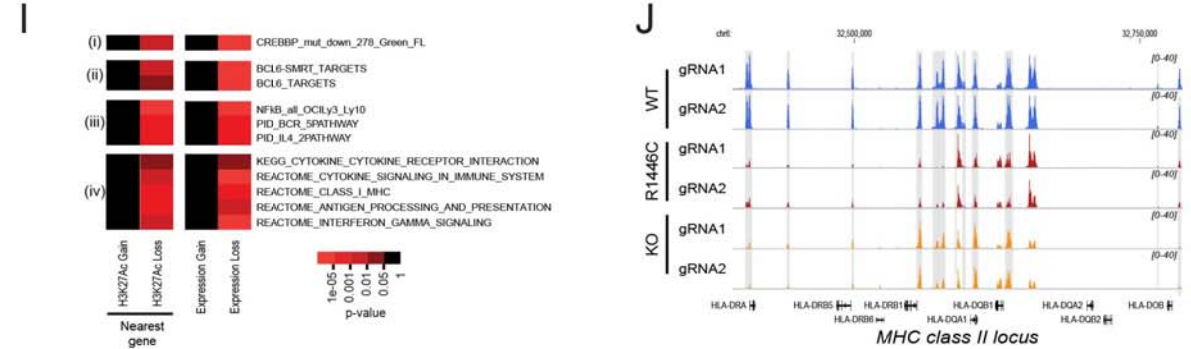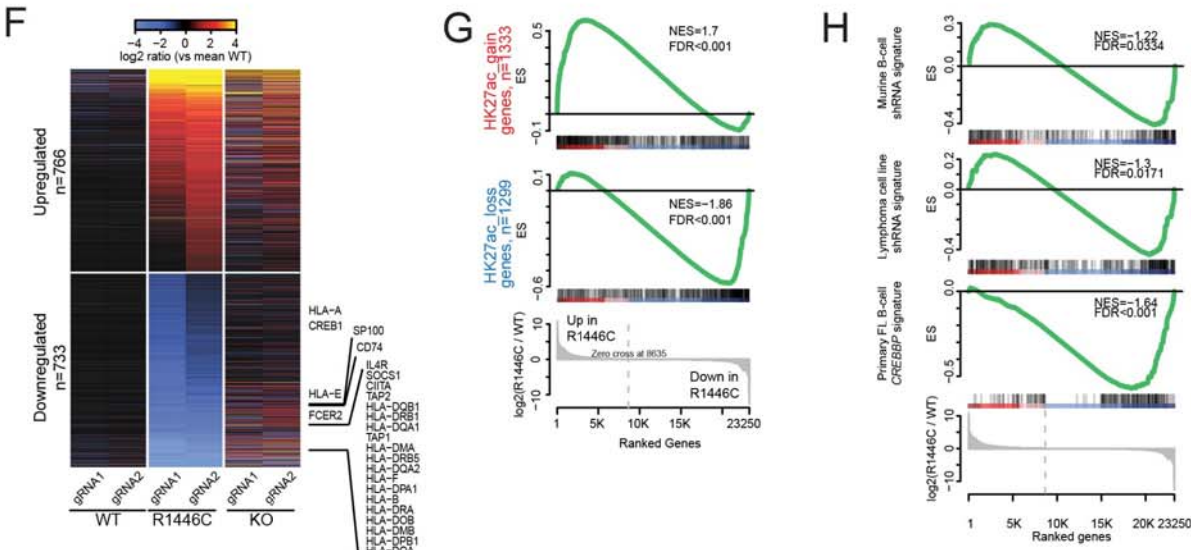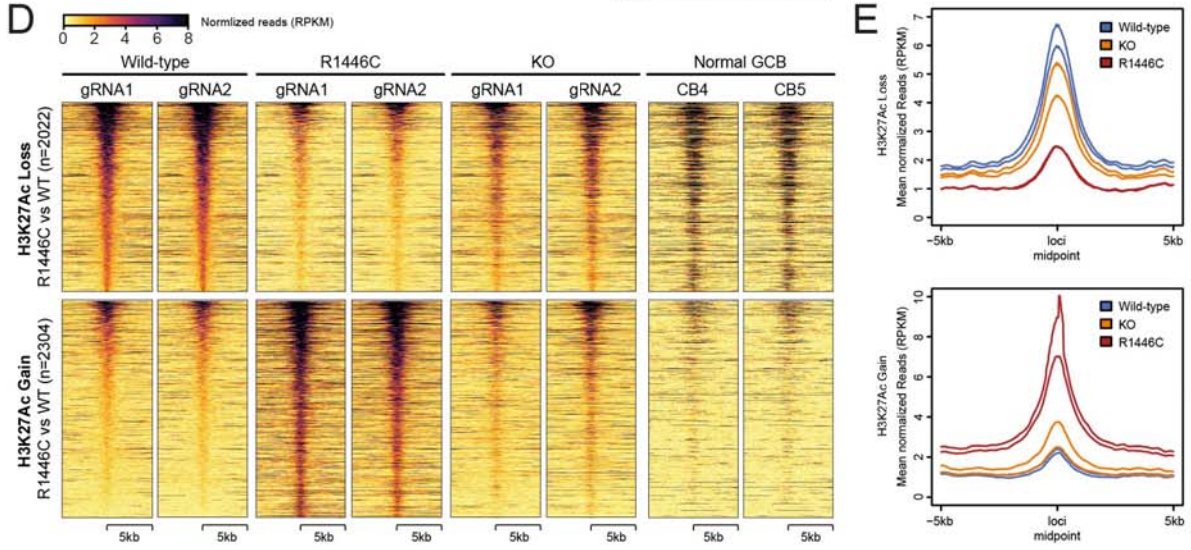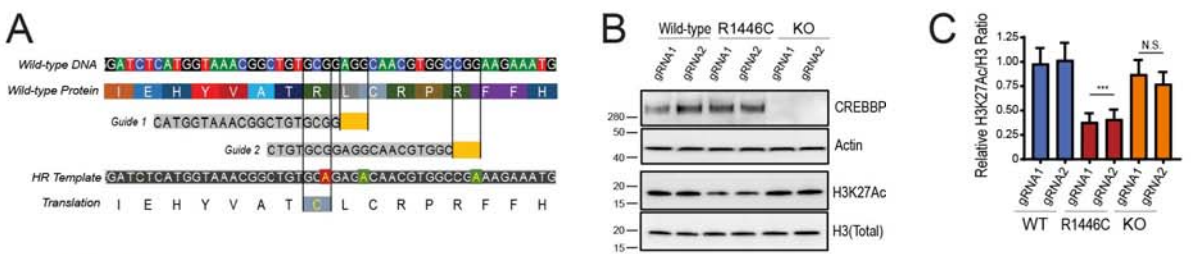1204
1205
1206
1207
1208
1209

1210 **Figure 6: Induction of interferon-responsive and antigen presentation genes in**
1211 **DLBCL cell lines and patient-derived xenograft. A)** A heat map shows significantly up-
1212 regulated (above) and down-regulated (below) genes in BRD3308-treated DLBCL cell
1213 lines that are *CREBBP* wild-type (OCI-Ly1) or mutant (OCI-Ly19 and OZ), expressed as
1214 a log2 ratio to vehicle control treated cells. The observed changes were consistent
1215 between wild-type and mutant cell lines, and included up-regulation of interferon-
1216 responsive and antigen presentation genes. **B)** MHC class II was assessed on vehicle
1217 control (left) and BRD3308 treated (25mg/kg, right) tumors from a *CREBBP R1446C*
1218 mutant PDX model, showing a visible increase in expression in the BRD3308-treated
1219 tumors. These images are representative of 4 tumors per group. **C)** An MHC class II-
1220 negative DLBCL patient derived xenograft model was treated *in vivo* with either 25mg/kg
1221 or 50mg/kg of BRD3308. Immunohistochemical staining was performed for MHC class II,
1222 revealing a robust induction of MHC class II expression that was relative to the dose of
1223 treatment. These images are representative of 6 tumors per group. **D)** qPCR was used
1224 to validate the gene expression changes of select interferon-responsive genes following
1225 BRD3308 treatment across an extended panel of *CREBBP* wild-type and mutant DLBCL
1226 cell lines. These genes were uniformly increased in both genetic contexts, but with a
1227 higher magnitude of increase in *CREBBP* mutant cell lines. One-tailed Students T-test
1228 *P<0.05, **P<0.01, **P<0.001. **E)** The induction of MHC class II expression by BRD3308
1229 was measured in an extended panel of DLBCL cell lines by flow cytometry. Data are
1230 plotted as a fold-change of the mean fluorescence intensity (MFI) of HLA-DR in
1231 BRD3308-treated vs control-treated cells. We observed uniformly increased MHC class
1232 II expression in all cell lines, but with higher magnitude in *CREBBP* mutants.
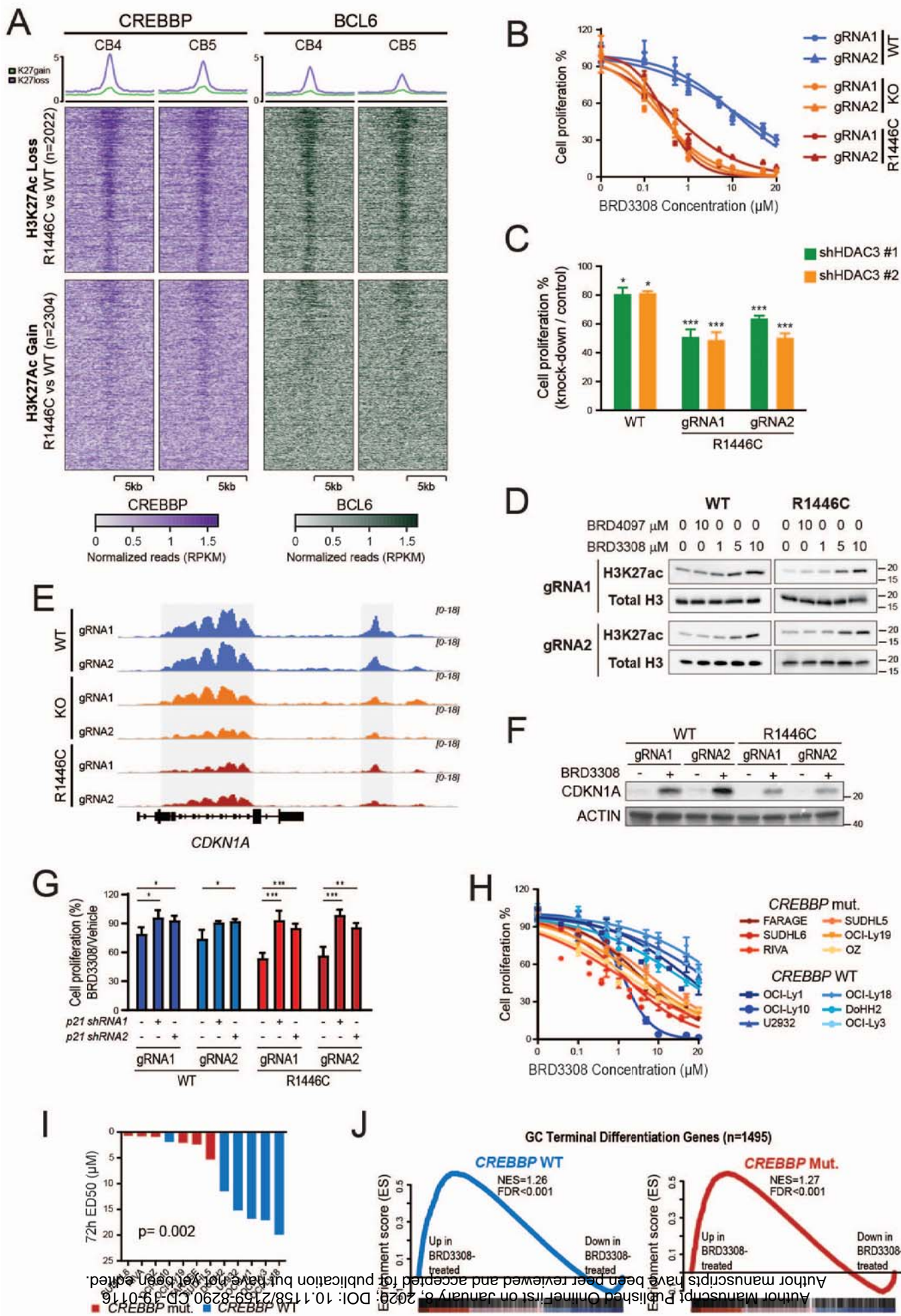1233
1234
1235
1236
1237
1238
1239
1240
1241
1242
1243
1244
1245
1246
1247
1248
1249
1250
1251
1252
1253
1254

1255 **Figure 7: HDAC3 inhibition induces antigen-dependent immune responses. A)** A
1256 schematic of the generation of antigen-specific T-cells and epigenetic priming of DLBCL
1257 cells. A human DLBCL cell line (OCI-Ly18) was engrafted into immunodeficient mice and
1258 allowed to establish. Human T-cells were then engrafted, exposing them to tumor
1259 antigens prior to harvesting of the tumor-infiltrating T-cell (TIL) fraction. These TILs were
1260 cultured with fresh DLBCL cells that had been epigenetically primed with different
1261 concentrations of BRD3308, and the cell viability of the DLBCL cells measured after 72h.
1262 **B)** TIL and DLBCL co-culture resulted in activation of the CD4 T-cells in a dose-dependent
1263 manner, as measured by flow cytometry for the CD69 activation marker. Data represent
1264 the fold change in CD69 expression compared to vehicle treated DLBCL cells (T-test vs
1265 DMSO control, *P<0.05). **C)** The cell viability of DLBCL cells in TIL co-culture experiments
1266 was measured by CellTiterBlue assay. Treatment with BRD3308 resulted in some cell
1267 killing through cell-intrinsic mechanisms in the absence of TILs (black). The addition of
1268 TILs at a 1:1 ratio led to a significant increase in cell death of the DLBCL cells. This was
1269 partially reduced by blocking of either MHC class I or MHC class II using neutralizing
1270 antibodies. Blocking of MHC class I and class II together completely eliminated the TIL-
1271 associated increase in cell death, suggesting that killing was mediated through MHC:TCR
1272 interactions. (T-test, *P<0.05, ***P<0.001) **D)** The production of IFN-γ was measured by
1273 ELISPOT and found to increase in cultures with epigenetically-primed DLBCL cells. (T-
1274 test vs DMSO control, **P<0.01, ***P<0.001) **E)** A syngeneic BCL6-dependent lymphoma
1275 model for *in vivo* testing of BRD3308 and PD-L1 blocking antibodies. Splenocytes were
1276 taken from $Ezh2^{Y641}$ x $I\mu Bcl6$ mice and injected into irradiated wild-type recipients that
1277 were treated upon the onset of lymphoma. **F)** Serum IFN-γ levels measured in mice
1278 following treatment. **G-N)** Representative immunofluorescence images of mouse spleens
1279 following treatment and quantification of mean fluorescence intensities from multiple mice
1280 for CD8 (G, H), CD4 (I, J), PD-L1 (K, L) and B220 (M, N), showing increased T-cell
1281 infiltration following treatment with BRD3308 and cooperation with αPD-L1 in eliminating
1282 B220+ tumor cells within the spleen. (T-test; *P<0.05, **P<0.01, ***P<0.001)

Figure 1

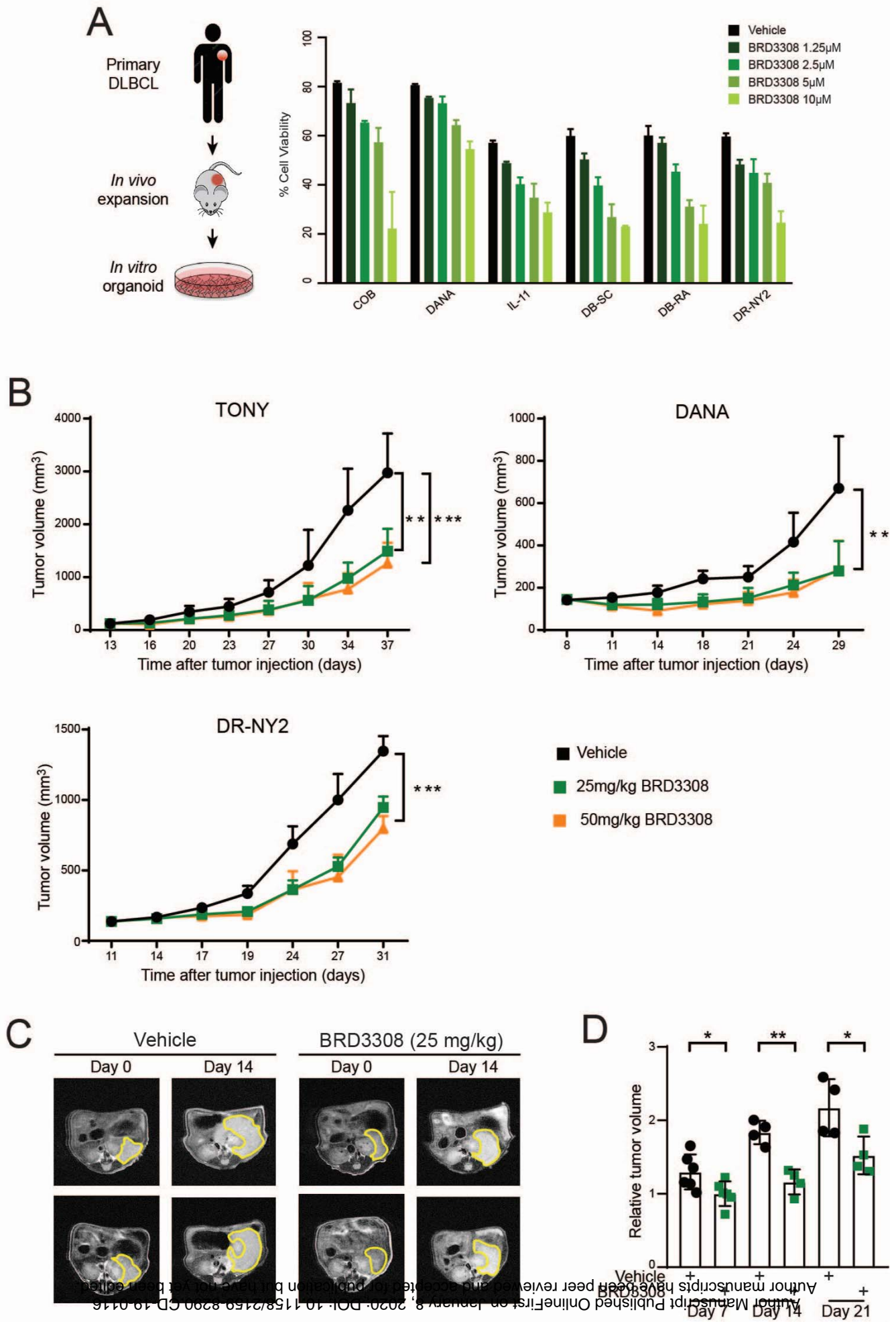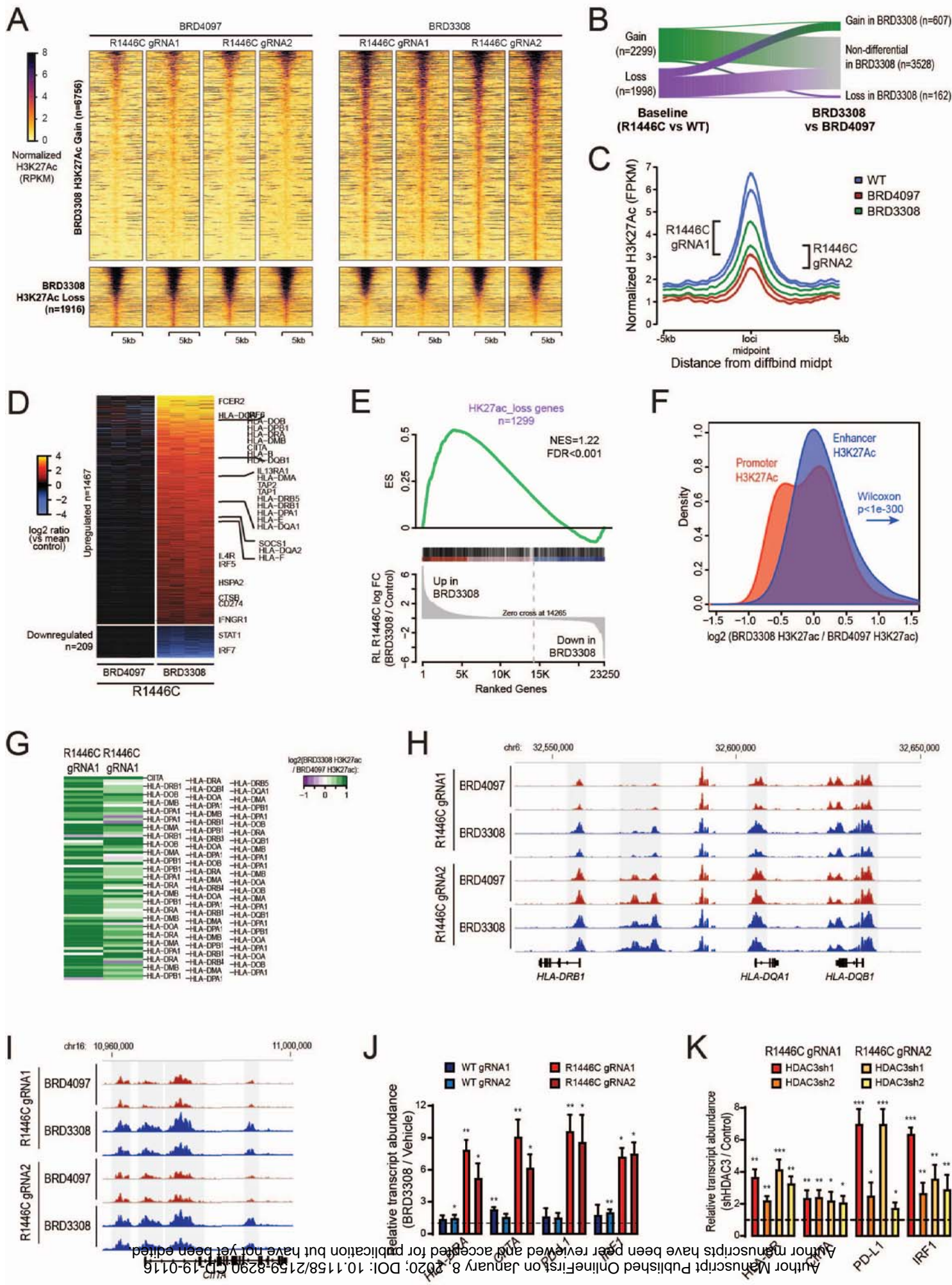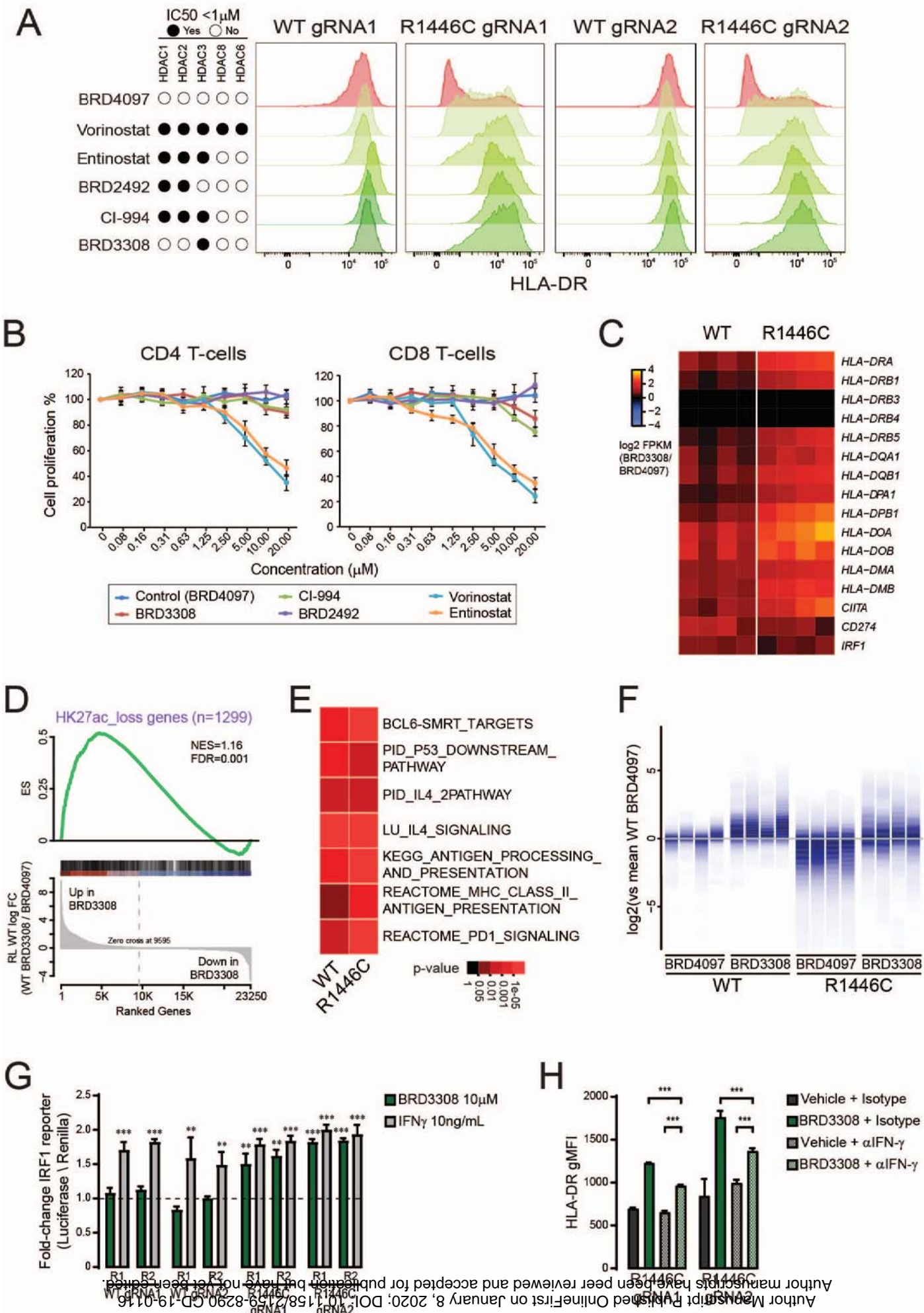
Author Manuscript Published OnlineFirst on January 8, 2020; DOI: 10.1158/2159-8290.CD-19-0116

Author manuscripts have been peer reviewed and accepted for publication but have not yet been edited.
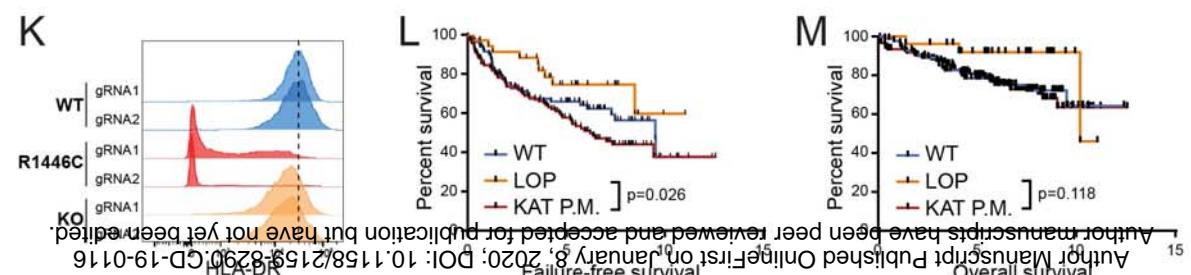
Figure 2

Figure 4

Figure 5

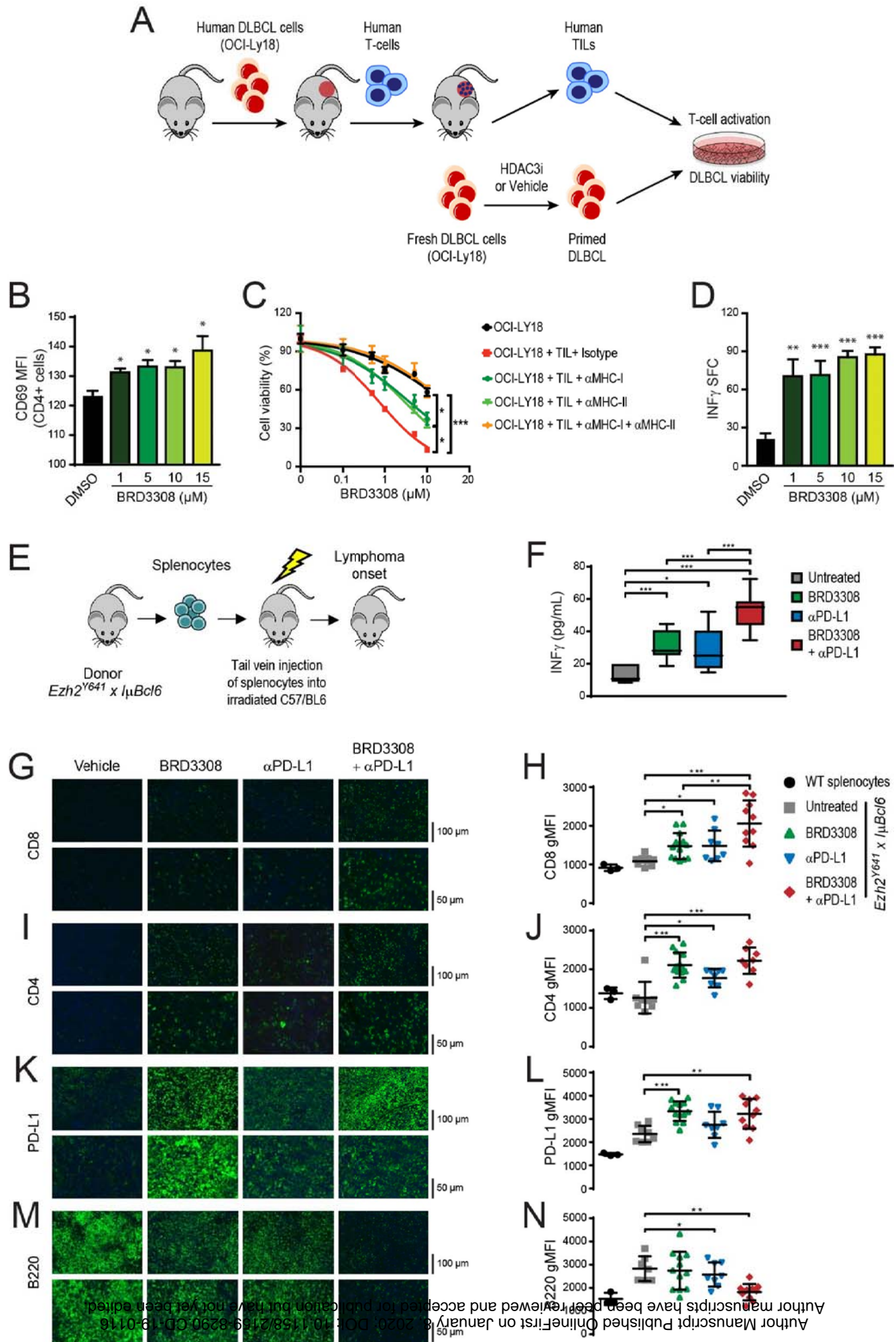# Figure 6
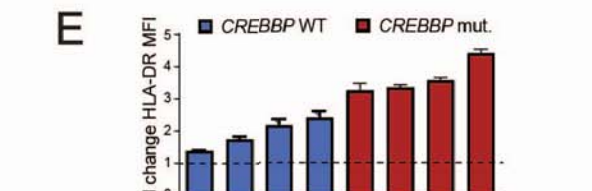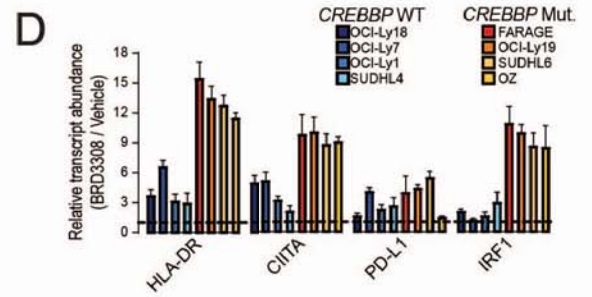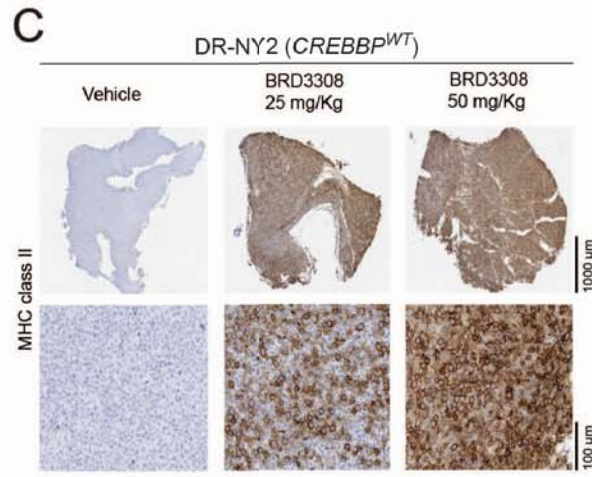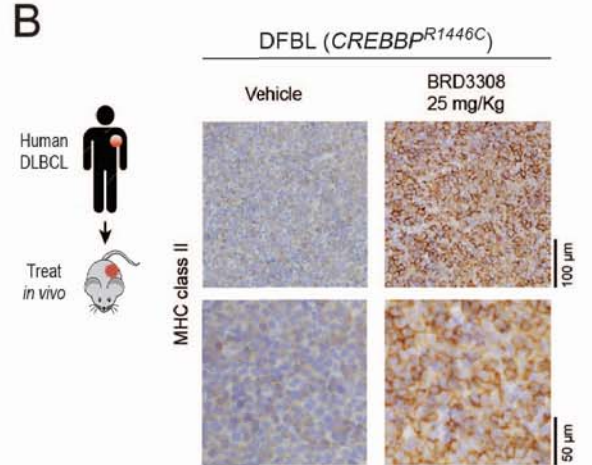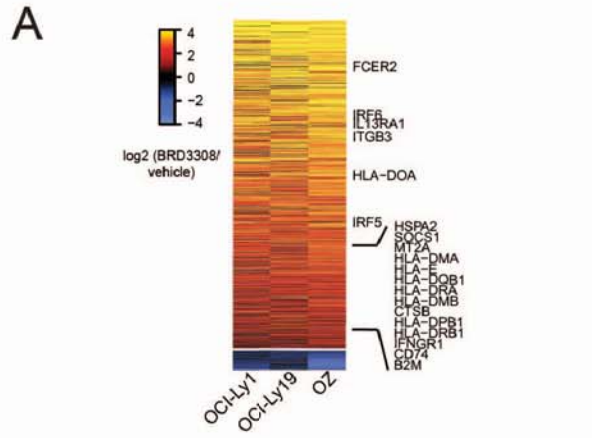
Figure 7

CANCER DISCOVERY

AACR American Association for Cancer Research

Selective inhibition of HDAC3 targets synthetic vulnerabilities and activates immune surveillance in lymphoma

Patrizia Mondello, Saber Tadros, Matt Teater, et al.

Updated version	Access the most recent version of this article at: doi:10.1158/2159-8290.CD-19-0116
Supplementary Material	Access the most recent supplemental material at: http://cancerdiscovery.aacrjournals.org/content/suppl/2020/01/07/2159-8290.CD-19-0116.DC1
Author Manuscript	Author manuscripts have been peer reviewed and accepted for publication but have not yet been edited.

E-mail alerts	Sign up to receive free email-alerts related to this article or journal.
Reprints and Subscriptions	To order reprints of this article or to subscribe to the journal, contact the AACR Publications Department at pubs@aacr.org.
Permissions	To request permission to re-use all or part of this article, use this link http://cancerdiscovery.aacrjournals.org/content/early/2020/01/07/2159-8290.CD-19-0116. Click on "Request Permissions" which will take you to the Copyright Clearance Center's (CCC) Rightslink site.